AD-A135 873 AN INTENSE EXCITATION SOURCE FOR HIGH POWER (BLUE-GREEN) LASER(U) HAMPTON INST VA DEPT OF PHYSICS AND ENGINEERING STUDIES K S HAN 22 NOV 83 1/2

UNCLASSIFIED ARO-17633.1-PH-H DAAG29-80-G-0014 F/G 20/5 NL

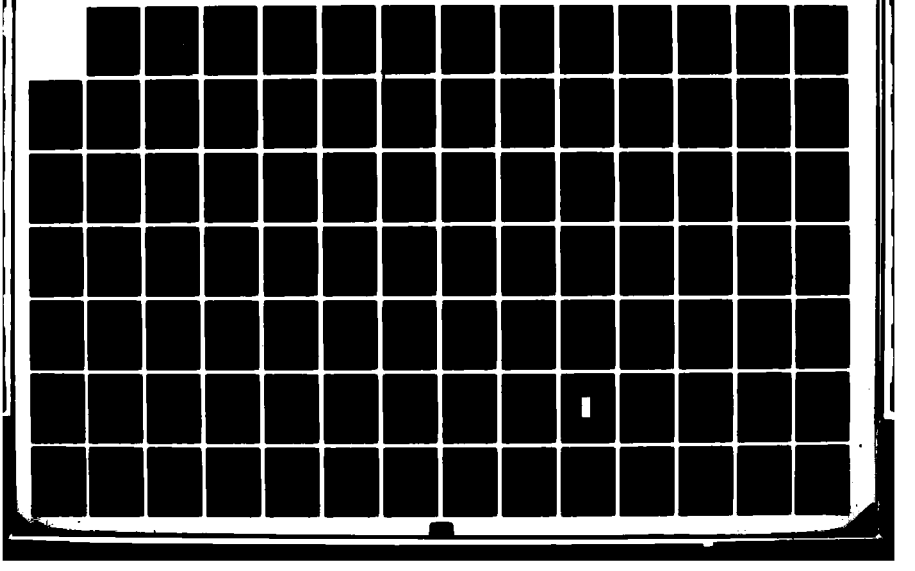

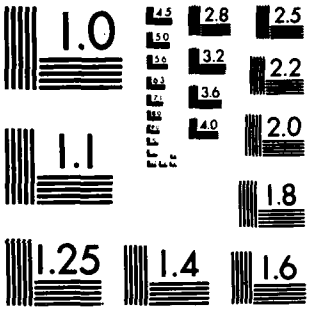

MICROCOPY RESOLUTION TEST CHART
NATIONAL BUREAU OF STANDARDS-1963-A

SECURITY CLASSIFICATION OF THIS PAGE (When Data Entered)

REPORT DOCUMENTATION PAGE

READ INSTRUCTIONS BEFORE COMPLETING FORM

1. REPORT NUMBER: 17633.1-PH-H; 18668.2-PH-H	2. GOVT ACCESSION NO. AD-A135873
3. RECIPIENT'S CATALOG NUMBER	
4. TITLE (and Subtitle): An Intense Excitation Source for High Power (Blue-Green) Laser	5. TYPE OF REPORT & PERIOD COVERED: Final Report 9/25/80 9/10/83
	6. PERFORMING ORG. REPORT NUMBER
7. AUTHOR(s): Kwang S. Han	8. CONTRACT OR GRANT NUMBER(s): DAAG29-80-G-0014 " 81 G 0014
9. PERFORMING ORGANIZATION NAME AND ADDRESS: Hampton Institute, Department of Physics and Engineering Studies, Hampton, VA 23668	10. PROGRAM ELEMENT, PROJECT, TASK AREA & WORK UNIT NUMBERS
11. CONTROLLING OFFICE NAME AND ADDRESS: U. S. Army Research Office, Post Office Box 12211, Research Triangle Park, NC 27709	12. REPORT DATE: November 22, 1983
	13. NUMBER OF PAGES: 93
14. MONITORING AGENCY NAME & ADDRESS(if different from Controlling Office)	15. SECURITY CLASS. (of this report)
	15a. DECLASSIFICATION/DOWNGRADING SCHEDULE

16. DISTRIBUTION STATEMENT (of this Report)

Approved for public release; distribution unlimited.

17. DISTRIBUTION STATEMENT (of the abstract entered in Block 20, if different from Report)

DEC 14 1983

A

18. SUPPLEMENTARY NOTES

THE VIEW, OPINIONS, AND/OR FINDINGS CONTAINED IN THIS REPORT ARE THOSE OF THE AUTHOR(S) AND SHOULD NOT BE CONSTRUED AS AN OFFICIAL DEPARTMENT OF THE ARMY POSITION, POLICY, OR DECISION, UNLESS SO DESIGNATED BY OTHER DOCUMENTATION.

19. KEY WORDS (Continue on reverse side if necessary and identify by block number)

Blue-Green dye laser, Hypocycloidal-pinch plasma as an intense excitation source for laser.

20. ABSTRACT (Continue on reverse side if necessary and identify by block number)

A high power blue-green dye laser has been pumped with an array of hypocycloidal-pinch (HCP) plasmas. The HCP pump source was energized by up to 4.2kJ energy stored in the capacitor bank. High pressure optical conversion. The maximum argon pressure used was 100 Torr with the optimum at 20 Torr. The rise time (≈1μs) of pumping light is kept short by using a small (6μF) capacitance. The laser output power and energy dependence of the input electrical energy, the type of gas, the filling pressure and the laser cavity parameters were studied with respect to the characteristics of the pumping light. The plasma temperature

DD FORM 1 JAN 73 1473 EDITION OF 1 NOV 65 IS OBSOLETE

SECURITY CLASSIFICATION OF THIS PAGE (When Data Entered)

20. ABSTRACT Cont.

7,250°K was obtained when the HCP was operated for the optimum laser output. The spectral efficiency of the absorbed radiation at this temperature was 22% or 83% of the maximum efficiency of the optimum blackbody source. We concluded that the HCP source has uv-rich spectrum, which can be varied to match the most efficient spectrum for laser pumping, and very high input capability. Thus it is suitable for repetitive and high average power laser systems.

A-1

TECHNICAL REPORTS

1. "Dye Laser Pumped by Hypocycloidal Pinch (HPC) Discharge."
   K. S. Han, C. H. Oh, D. D. Venable, J. H. Lee
   IEEE82CH1479-1, page 182. (1982)
2. "Near uv Emission of Hypocycloidal-pinch (HCP) Discharge."
   K. S. Han, D. K. Park, D. D. Venable, J. H. Lee
   Technical Report No. 2, 1982.
   Bull of APS. Vol 27, 1063 (1983)
3. "Optical Pumping Blue-green Laser by Hypocycloidal-pinch Plasma:
   K. S. Han, S. H. Nam, J. H. Lee
   Submitted in Journal of Applied Physics for Publication on Oct. 20, 1983.
4. "Radiative Properties of Hypocycloidal Pinch Plasma for Optically Pumped Blue-Green Lasers."
   K. S. Han, M. Niimuva, S. T. Ko, J. H. Lee
   To be submitted in Journal of Applied Physics for Publication on Dec. 1983.
5. High Pressure Plasma Source for Atomic Iodine Lasers.
   K. S. Han, D. K. Park, J. H. Lee
   To be submitted in Journal of Applied Physics for Publication on Dec. 1983.

Scientific personnel involved under ARO Grant (DAAG29-81-G-0014) are

		Period
K. S. Han	(Principal Investigator)	October 1, 1982 - Present
J. H. Lee	(Faculty Associate and Adjunct Prof. of Physics)	October 1, 1982 - Present
M. Niimura	(Research Associate)	October 1, 1982 - Present
D. K. Park	(Research Associate)	October 1, 1981 - September 30, 1982
*S. H. Nam	(Graduate Student) Completed M. S. Thesis December 1983	June 1, 1982 - September 30, 1983
*S. T. Ko	(Graduate Student) Completed M. S. Thesis December 1983.	June 1, 1982 - September 30, 1983

*Present Address: Old Dominion University, Department of Electrical Engineering, Norfolk, Virginia 23605.

Final Technical Report

Under

ARO Grant No. DAAG29-80-G0014

An Intense Excitation Source of High Power Laser

Nov. 20, 1983

Principal Investigator

K. S. Han

Hampton Institute

Department of Physics and Engineering Studies

Approved for Public Release

ABSTRACT

A high power dye laser using LD490 and Rh6G has been successfully pumped with a multiple array of hypocycloidal pinch (HCP) plasmas. Laser excitation was achieved for the first time with high-pressure heavy gases (Xe, Ar) in the HCP device. Up to 230 kW of blue-green laser outputs were measured.

The untuned peak wavelength of the blue-green laser with LD490 is 503.5 nm and the maximum output energy density is 40 mJ/cm^3. The length of the laser pulse (FWHM) is ~1 μs. A maximum overall efficiency of 0.012% is achieved.

The laser output characteristics are studied in this experiment for the type of gas, the filling gas pressure and the laser cavity parameters. The spectral distributions of laser output, fluorescence, absorption and pumping light are also studied. The spectral radiation of the HCP source shows good spectral match with the absorption spectrum of LD490. Therefore, the laser output power obtained with LD490 was higher than with Rh6C. Consequently, the HCP array is very attractive to pump blue-green lasers compared with the conventional flashlamps.

Spectral efficiencies of blackbody and bremsstrahlung emissions are theoretically studied to compare the emission of the HCP array. The maximum efficiencies obtainable are 26.46% at the temperature of 9750 K for blackbody radiation and 13.84% at 38,500 K for bremsstrahlung emission. The measured color

temperature of the HCP array is 7,250 K when a blackbody emission is assumed. The spectral efficiency for this temperature is 22.08% or 83.45% of the maximum efficiency obtainable from blackbody radiation.

ACKNOWLEDGEMENT

I would like to express sincere gratitute to the following persons for making this research project successful: Mr. S. H. Nam. and Dr. J. H. Lee.

This work was supported by Army Research Office Grant No. DAAG29-80-G0014.

TABLE OF CONTENTS

TABLE OF CONTENTS (CONTINUED)

LIST OF TABLES

LIST OF FIGURES

LIST OF FIGURES (CONTINUED)

CHAPTER I

Introduction

A. Background

Dyes are more attractive than other gain media for producing a laser that is easily tunable over a wide range of wavelengths. Dyes can be used in the solid, liquid, or gas phases and their concentration, and hence their absorption and gain, is readily controlled. Also, the cost of the active medium, organic dyes, is negligibly small compared to that of others. Early speculations about the use of organic compounds (Refs. 1 and 2) produced correct expectations of the role of vibronic levels of electronically excited molecules (Ref. 3), but the first experimental study that might have led to the realization of an organic laser was by Stockman (Ref. 4) et. al. and Stockman (Ref. 5). Using a high-power flashlamp to excite a solution of perylene in benzene between two resonator mirrors, Stockman found an indication of a small net gain in his system. In 1966, Sorokin and Landard (Ref. 6) at IBM's Thomas J. Watson Research Center, Yorktown Heights, were the first to obtain stimulated emission from an organic compound, namely chloro-aluminum-phthalocyanine. Stimulated emission from phthalocyanine compounds, eryptocyanine and methylene blue was reported in 1967 by Stapanov and coworkers (Refs. 7 and 8). Today dyes cover the range from 340 nm- 1 micron. The most efficient dyes are in visible region, generally running between 460 nm to about 660 nm.

In particular the blue-green laser has a low absorption coefficient in water (Ref. 9), and it is the best candidate for underwater communi-

cation where high pulse energy is of primary importance. Usually the flashlamp pumped dye laser is considered for this application. The copper vapor laser is the best immediate choice for underwater range-gated application, where 5-20 nanosecond pulses are needed. A single pulsed laser that is suitable for both applications is not yet available. A cw laser with reasonable efficiency is also unavailable. Of all the flashlamp pumped dye laser pumping configurations that have been demonstrated to date, only the vortex stabilized flashlamp configuration offers the operational lifetime ($>10^7$ shots) and high average power capabilities (>10 watts) required for most ocean optics applications. The goal for ocean optics is to define a device with the characteristics of Table 1 (Ref. 10). However, there is no system which outperforms these requirements to date.

A natural step to follow in developing dye lasers was the development of laser pumping light sources. The flashlamps comparable in rise-time and intensity to giant-pulse ruby lasers enabled dye lasers to be pumped with a convenient, incoherent light source. Xenon flashlamps have been commonly used as the pumping light source for liquid dye lasers. Other pumping light source have been tried for liquid dye lasers, but these have not been shown to be better pump sources than flashlamps (Ref. 10). However, flashlamps have some disadvantages for high power operation. At optimum operation, the volume of the lamp is completely filled with the discharge. The rapidity and uniformity of the discharge is attributed to photoionization of the fill gas. For this optimized operation of a flashlamp laser system, there are serious limitations in the system that could not be overcome. Localized line

Table 1

Goal and Achievement for Ocean Optics

	Goal	Achieved in the Experiment
Output energy per pulse	50 millijoule	163 millijoule
Pulse length	0.5 microseconds	~ 1 microseconds
Pulse amplitude stability	± 5%	---
Operational life	> 20 hours	> 20 hours
Output wavelength	490 30 nanometer	503.5 nanometer
Output bandwidth	< 10 angstrom	70 angstrom
Power consumption	< 10 kilowatts	< 10 killowats
Size	< 24 cubic feet	< 24 cubic feet
Weight	< 550 pounds	---

discharges or filaments always form so that the discharge volume is not completely filled. In addition, the nonuiform pumping of the dye cell produces an undesirable profile of laser beams and reduces the optical coupling efficiency. Also the relatively large inductance of the xenon flashlamp leads to slow rise time in current. The rise time of current is typically 140 nanoseconds for energies below 100 joule. The maximum electron or plasma temperature of the discharge is in the neighborhood of 2.5-3.0 eV (Ref. 11). This plasma temperature of the flashlamp cannot be raised by increasing either the discharge current or the filling gas pressure. The input energy is limited by the fact that the 25,000 K blackbody radiation should not load the envelope significantly in times of a few microseconds (Ref. 11). Therefore, clustered linear flashlamps for dye laser excitation which has a number of potential advantages over competitive pumping techniques has been used. Furthermore, several dye capillaries, each with its own linear flashlamp to realize a single system that can produce either high energy-per-pulse at low pulse repetition rates or low energy-per-pulse at high pulse repetition rates have been used (Ref. 10). The primary disadvantages of the clustered flashlamp pumping geometry are that flashlamp lifetime is limited by wall erosion and electrode sputtering to fewer than 10^6 shots and the efficiency is characteristically quite low. Workers at Naval Electronics Laborabory Center succeeded in producing 50 millijoule pulses (on a single shot basis) from a double capillary clustered flashlamp system. An efficiency of 0.25% was reported (Ref. 10).

Recently, the intense ultra-violet emission from a dense plasma focus apparatus was studied, and advantages in power output, life

expectancy and availability of spectral selections in the UV, vacuum-UV, and soft X-ray region have been recognized (Ref. 12). This device has also been proved to be useful for visible spectral emission which is suitable for pumping high power dye lasers. This geometry is called a hypocycloidal-pinch or HCP and was originally developed for production of plasmas with parameters characteristic of thermonuclear fusion reactors (Ref. 13). The successful pumping of an iodine photodissociation laser at 1.315 μm and a xenon recombination laser at 2.027 μm using the hypocycloidal-pinch array have been reported (Ref. 13). Also laser activity from a dye (rhodamine 6G) by using a double unit array of HCP as the exictation light source has been reported (Ref. 14). By using the HCP device, a plasma electron temperature, T_e, of 1 keV and a plasma density, n_e, of 10^{19} cm^{-3} have been achieved (Ref. 15). However by changing the operating conditions, such as filling gas pressure, gas species, input energy and the HCP geometry, it is possible to lower T_e and n_e to the ranges apprximately 1 eV and 10^{18} cm^{-3}, respectively. Expecially, the multiple unit array of HCP which renders a long gain length is suitable for pumping a blue-green dye laser at the power level appropriate for the underwater communications.

Recently a low power blue-green dye laser has been indeed pumped with an array of HCP (Ref. 16). A low pressure-light gas regime of HCP operation was used and consequently the laser output was limited to 10 mJ per pulse at an efficiency of 10^{-4}%. When a few torr of heavy gas, Xe, was used they failed to obtain laser action due to the slow rise time of the pump light even though the heavy gas produced higher energy light pulses than that of the other gases tested - such as deuterium,

helium and nitrogen. This slow rise time (>2 μs) may come from the large capacitance (86 μF) they used for the system.

B. Purpose of the Project

The purpose of this project is to develop a new pumping light source for dye lasers by using a hypocycloidal-pinch (HCP) array which may enhance the output power level of pulsed blue-green dye lasers. Demonstration of high power capability, durability of the system as well as characterization of the HCP plasma as a dye laser source are the major objectives of these experiments.

The following are subjects of investigation for the purpose:

1. Laser output power or energy as a function of filling gas pressure in HCP (argon, xenon and helium);
2. Laser output energy dependence on output coupling;
3. Laser output power as a function of number of shots;
4. Laser output energy as a function of the dye concentration;
5. Laser output energy as a function of input energy;
6. Spectroscopic analysis of the pumping light of HCP;
7. Lasing spectrum and fluorescence spectrum of dye LD490;
8. Absorption spectrum of dye LD490; and
9. Spectral efficiency of radiation for pumping LD490.

CHAPTER II

Description of Theory

A. Hypocycloidal-pinch Plasma as a Laser Pump Source

Figure 1 shows the cross section of the hypocycloidal pinch apparatus used for dye laser pumping. The device consists of eight brass electrodes. One can visualize this geometry as formed by the cross section of the coaxial plasma focus apparatus rotated about an axis, Z, positioned in front of and perpendicular to the electrodes. In contrast to the normal practice which forms an HCP array by parallel connections (see Refs. 12, 13 and 15), a series connection is used here. The series connection increases the impedance of the HCP array and correspondingly more electrical energy is dissipated in the device than would be for a parallel connection. As shown in the figure, the eight electrodes are connected in series with four chains of resistors. Each resistor chain consists of seven resistors resulting a total of twenty-eight resistors. When the switch is triggered, the currents flow through the resistor chains for a very brief period of time providing voltage divisions for each electrodes. Due to this divided voltage applied on the electrodes, gas breakdown occurs over the insulator surfaces simultaneously. The insulators which were made of ceramic glass (Macor) and placed between the electrodes are in the form of a disk, but have a decreased thickness toward the center hole so that the shadow effect of the electrodes could be minimized. Once gas breakdown is achieved at the insulator surface, the current buildup causes the current sheet to more radially outward in

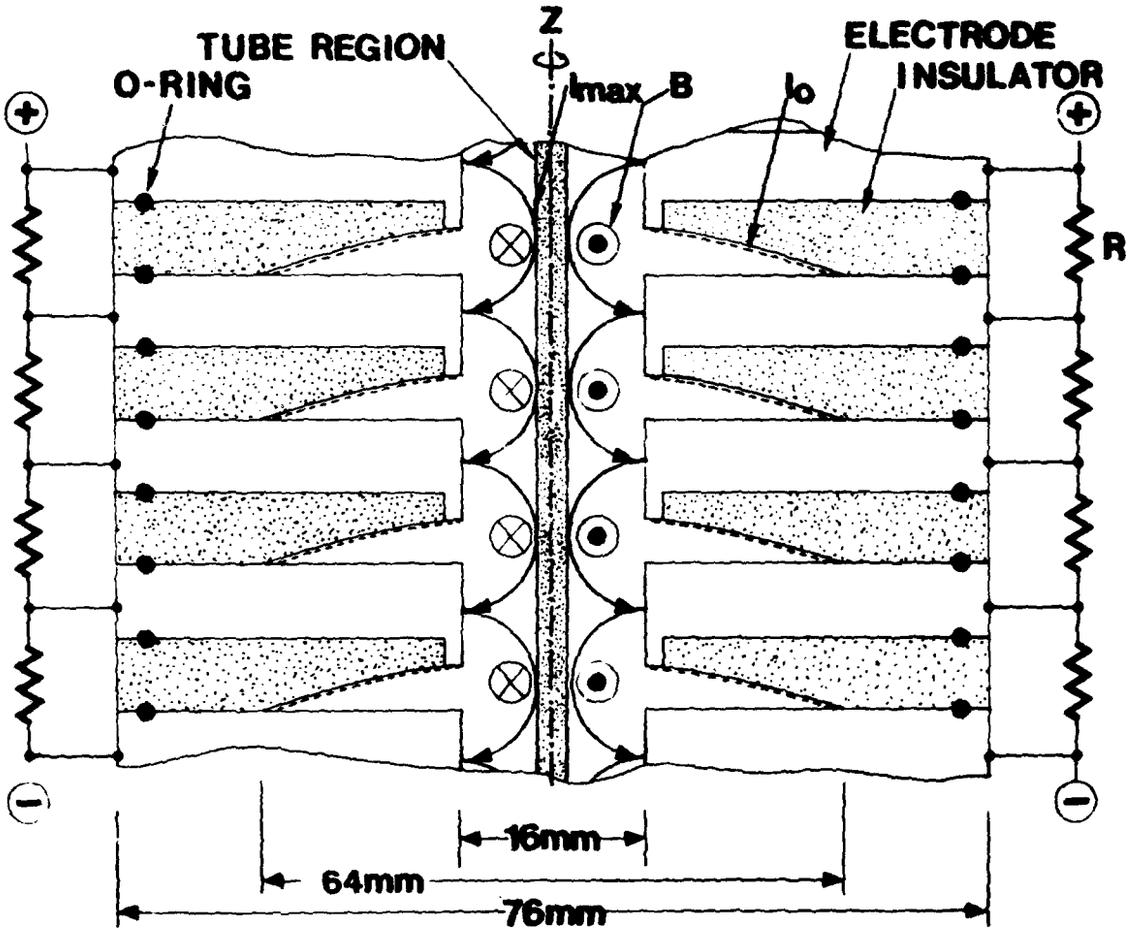

FIGURE 1. CROSS SECTIONAL VIEW OF THE HYPOCYCLOIDAL PINCH APPARATUS (HCP).

an inverse pinch mechanism by the action of the $\vec{J} \times \vec{B}$ force, forming a parabolic current sheet over the insulator surfaces. The current sheets subsequently accelerated toward the center hole until they collapse into the hole. The collapse of the current sheets makes two types of plasma modes depending on the filling gas species and pressures (Ref. 13). The first is a heavy gas-high pressure plasma mode and the second is a light gas-low pressure plasma mode. In the latter case, the current sheets launched from the insulators advance radially toward the center hole and form strong pinches around the axis of the apparatus. These pinches produce several plasma foci. In the former case, the collapse of current sheets is mild and forms plasma rings near the edges of the center holes as indicated by the circular line in Figure 1. For dye laser pumping, the high pressure mode is preferred to the low pressure mode because it is easy to insert a dye cuvette along the axis of the apparatus without disturbing the plasma-ring formation, and the heavy gas plasmas produce more high-intensity light pulses than light gas. It is also possible to adjust the diameter of plasma rings by changing the impedance of the circuit, the rundown distance, and the filling pressure.

The following seven phases of the discharge occurs in the dynamics of the hypocycloidal-pinch:

1. Voltage division at the electrodes through resistors;
2. the inverse pinch over the insulator at the beginning of the discharge;
3. the rundown of the current sheets as a result of the $\vec{J} \times \vec{B}$ force toward the center hole;

4. the collapse of the current sheets into the center hole;
5. the formation of plasma rings;
6. the expansion and radiative cooling of the plasma which results in
7. the intense emission of radiation in the ultra-violet, visible and infrared ranges.

The HCP array used in the experiment has a rundown radius of 32 mm with a 16 mm diameter center hole. The space between electrodes is 6.4 mm. An O-ring is positioned between the electrode and the insulator in order to make vacuum sealed chambers which keep the filling gas. The impedance of this device varies rapidly from zero to the maximum value as the current sheets move toward the center hole. The dominant component of the impedance of the system is the inductive reactance. The maximum inductance of the device for one unit can be calculated by the following simple formula, assuming the current sheets as a coaxial path (see Figure 1).

$$L_{max} = (\mu_o\, h/2\pi)\, \ln\,(r_2/r_1)\ \text{(henrys)} \qquad (1)$$

where, μ_o; permeability, $4\pi \times 10^{-7}$ henrys/m

h; distance between electrodes, 6.4×10^{-3} m

r_1; radius of the plasma ring, 8×10^{-3} m

r_2; radius of the outer edge of the electrodes, 32×10^{-3} m.

The calculated value of the maximum inductance for one unit is 2.7 nH. Therefore, the total series inductance ($L_t = 7 \times L_{max}$) of the HCP array is 18.6 nH. This value is less than the inductance of the capacitor used

and extremely small when compared with a typical linear flashlamp. Only coaxial flashlamps may have comparable inductances. Therefore, it is desirable to have the HCP coupled with an extremely fast pulse power source for efficient operation although no effort was made to obtain such a power source for this experiment.

B. Dye Laser Kinetics

In the energy levels of a typical dye molecule in solution as shown in Figure 2, there are a manifold of singlet electronic states, G, S1, S2 and triplet states T1 and T2. For most purposes, dye lasers can be described by these five electronic energy states and the transitions between these states. Each of the electronic states is very wide in energy, being broadened by a continuum of vibrational, rotational, and solvent states. This continuum gives rise to the characteristically broad, structureless absorption and emission bands in the electronic spectra of dye molecules in solution. If the ground state G of the molecule is in a thermal equilibrium with its surroundings at room temperature, most of the molecules are in the lowest vibrational level of G. Thus in the absorption process, the molecule is raised from the rotational-vibrational levels of the excited singlet states S1 and S2 in accordance with the Frank-Condon principle (Ref. 17). The molecular absorption cross section $\sigma^{o}(\lambda)$ is defined by the relation (Beer's Law)

$$I(L, \lambda) = I(0, \lambda)\, e^{-\sigma^{o}(\lambda)NL} \qquad (2)$$

where $I(0, \lambda)$ is the light intensity incident on an absorbing sample of length L, N is the molecular concentration (number of molecules $\cdot$ cm^{-3})

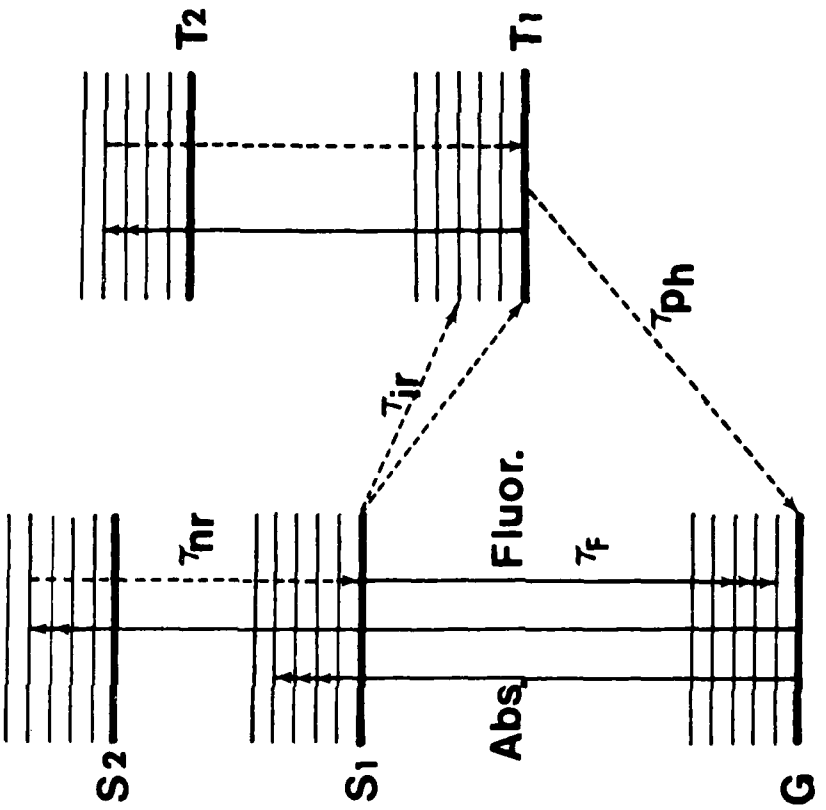

FIGURE 2. EIGENSTATES OF A TYPICAL DYE MOLECULE WITH RADIATIVE (SOLID LINES) AND NON-RADIATIVE (BROKEN LINES) TRANSITIONS.

and $I(L, \lambda)$ is the intensity of the transmitted beam. A convenient form for solutions to this equation is

$$I(L, \lambda) = I(0, \lambda) \cdot 10^{-\varepsilon(\lambda)ML} \qquad (3)$$

where M is the molar concentration and $\varepsilon(\lambda)$ is the molar decadic extinction coefficient (measured in litre $\cdot$ cm^{-1} $\cdot$ $mole^{-1}$). In terms of $\varepsilon(\lambda)$, $\sigma^{o}(\lambda) = 3.82 \times 10^{-21}\ \varepsilon(\lambda)$. Here $\sigma^{o}(\lambda)$ is given in units of cm^2 (Ref. 17).

Depending on the wavelength of excitation light, the molecule may be excited to the first excited singlet state, S1, or higher excited singlet states S2. The latter is the case for many laser dyes excited by UV pump sources. De-excitation of an excited dye molecule takes place through fluorescence emission or through various nonradiative processes. The process that is directly used in dye lasers is the radiative transition from the lowest vibronic level of the first excited singlet state, S1, to the ground state, G, for almost all dyes. The internal conversion between S2 (and higher excited states) and S1 is usually extremely fast, usually taking place in times on the order of 10^{-11} - 10^{-12} sec; vibrational relaxation in the S1 state also occurs in times on the order of picoseconds (Ref. 17). This is the reason why fluorescence process is generally independent of the initial electronic state, S2, or the initial vibronic state of S1 to which the molecule may be excited. If we compare these times with the lifetime of the S1 state, which is on the order of nanoseconds, these times are very short. Therefore, the fluorescence quantum efficiency, the fluorescence spectrum and the fluorescence lifetime of most dye molecules are independent of the wave-

length of excitation light. During the relaxation process, S2→S1, which is a nonradiative transition, the large amount of energy must be dissipated as heat. Therefore, in the comparison between the excitation processes G→S2 and G→S1 we see the disadvantage of the excitation process G→S2. Fluorescence (and hence stimulated emission) takes place from the lowest vibronic level of S1 to various vibrational-rotational levels of G. From here again, fast vibrational relaxation brings the molecule back to the lowest vibronic level of G. Therefore, it is obvious that the dye laser is in effect a four level laser system with all the four levels lying in the singlet manifold. But there are two other important processes. The first is intersystem crossing from S1→T1 and subsequent T1→T2 absorption at pump or laser wavelengths. Both these processes can have an influence on the performance of the dye laser.

As indicated earlier, stimulated emission originates from the lowest vibronic level of S1, and takes place to a vibronic level of G. Since the relaxation processes in the excited singlet states are so rapid, all the excited dye molecules have an equal probability of emitting to a given vibronic level of G. The emission cross-section $\sigma_e(\lambda)$ is given by the relationship (Ref. 17)

$$\sigma_e(\lambda) = \frac{\lambda^4 \cdot E(\lambda)}{8\pi \cdot \tau_f \cdot c \cdot n^2} \tag{4}$$

where $E(\lambda)$ is the fluorescence line shape function normalized such that

$$\int_0^\infty E(\lambda)\, d\lambda = Q_f \quad . \tag{5}$$

Q_f is the fluorescence quantum efficiency (or quantum yield), n is the

refractive index of the dye solution at wavelength λ, τ_f is the fluorescence lifetime (observed lifetime of the S1 state in the absence of stimulated emission) and c is the velocity of light. The many processes which tend to decrease Q_f can be grouped together into nonradiative processes occurring between states of the same multiplicity (internal conversion), and those occurring between states of different multiplicty (intersystem crossing). If K_g is the rate of internal conversion between S1 and G, and K_t the intersystem crossing rate from S1 to T1, then the quantum yield of fluorescence is (Ref. 18)

$$Q_f = \frac{1/\tau_{rf}}{K_g + K_t + 1/\tau_{rf}} \tag{5a}$$

and

$$Q_f = \frac{\tau_f}{\tau_{rf}} \tag{5b}$$

Finite values of K_g and K_t therefore lead to a decrease in Q_f. Intersystem crossing, in addition, populates the triplet states and results in subsequent T1→T2 absorption. This can cause a severe loss mechanism in dye lasers.

The gain coefficient of the dye laser medium at wavelength λ (in the absence of external losses) is defined as

$$g(\lambda) = \sigma_e(\lambda)\, N_1 - \sigma^0(\lambda)\, N_0 - \sigma^1(\lambda)\, N_1 - \sigma^t(\lambda)\, N_t \tag{6}$$

where N_0, N_1, N_t are the molecular population densities (molecules/cm^3) in the states G, S1 and T1, respectively; σ_e, σ^0, σ^1, σ^t are respectively the stimulated emission cross section, the G→S1/S2 absorption cross section, S1→S2 absorption cross section and the triplet-triplet

(T1→T2) absorption cross section. The three absorption processes which lead to a decrease in gain at a given wavelength λ are ground state absorption, excited singlet state absorption and triplet-triplet absorption.

Ground state absorption at lasing wavelengths is due to partial overlap of the fluorescence and absorption spectrum of the dye. If most of the dye molecules were excited to higher singlet states, the ground state absorption term $\sigma^{o}(\lambda)\ N_0$ would be small and the gain would have a maximum very near the peak of the fluorescence spectrum (in the absence of S1→S2 and T1→T2 absorption losses). For rhodamine 6G, the Stokes shift is small and the gain maximum does not generally occur at the peak of the fluorescence band. On the other hand, for some Coumarin dyes (blue laser dyes) which have large Stokes shift, the peak gain occurs at the wavelength of the fluorescence peak. In many dye laser systems, part of the active medium had to remain unpumped for constructional convenience. The unpumped solution acts as a passive absorber and causes a shift in the laser emission peak towards longer wavelengths. Coarse tuning methods such as concentration tuning, tuning by variation of the length of the active medium or by variation of pump power, all utilize ground state absorption (Ref. 17).

Molecules in the excited state S1 can absorb either pump or dye laser photons and go to higher excited singlet states S2 (Ref. 19). As mentioned earlier, rapid radiationless decay from S2 by a cascade of internal conversion and vibrational relaxation processes, brings the molecule back to the lowest vibrational level of S1. Therefore, excited state absorption does not in general cause an inversion loss. However,

the optical loss associated with excited state absorption of pump or laser photons does adversely affect the dye laser performance in many ways. Absorption at lasing wavelengths reduces the gain and efficiency of the laser. If $\sigma^1(\lambda) > \sigma_e(\lambda)$, the gain is negative and laser action cannot be obtained at wavelength λ. For $\sigma^1(\lambda) < \sigma_e(\lambda)$ laser action is possible but with reduced gain due to a lower effective stimulated emission cross section. At the pump wavelength, λ_p, the optical loss coefficient due to excited state absorptions is $\sigma_p^1(\lambda)\ N_1$, where $\sigma_p^1(\lambda)$ is the excited state absorption cross-section at the pump wavelength. This loss coefficeint increases with N_1. Another undesirable result of excited state absorption is that since the S2→S1 transition is radiationless, pump or laser photons absorbed by molecules in S1 reappear as heat in the dye solution, leading to deterioration in laser performance.

One of the earliest recognized problems associated with dye lasers was accumulation of molecules in the triplet state T1 and subsequent T1→T2 absorption. The radiative transition from T1→G transition is spin forbidden and hence the triplet state lifetime τ_p is relatively long (usually in the 10^{-7} ~ 10^{-3} sec range), depending on the environment of the dye (Ref. 19). It is possible to estimate the radiative lifetime, τ_{rp}, of the phosphorescence on the basis of the G→T1 absorption. Since this transition is normally completely obscured by absorption due to impurities, the phosphorescence radiative lifetime can be obtained from the quantum yield of phosphorescence, Q_p, and the observed phosphorescence lifetime τ_p: $\tau_p = Q_p\ \tau_{rp}$ (Ref. 18). The radiationless transition from an excited singlet state S1 to a triplet state T1 can be induced by internal perturbations as well as by external perturbations. Molecules

crossing over from S1 to T1 by intersystem crossing are trapped there and cannot participate in laser action. A much more serious consequence in that since triplet-triplet transitions are spin allowed, the relevant absorption corss-sections σ^t are large and for many dyes this absorption spectrum overlaps the S1→G fluorescence spectrum (Ref. 18). This leads to a reduction in gain.

Dye parameters for rhodamine 6G and LD490 are shown in Table 2. For LD490, only the available parameters are listed.

C. Rate Equations

A simple geometry of the HCP pumping configuration, as shown in Figure 3, is used for the rate equation calculations (Ref. 17). The laser resonator is made of the active medium of length L with two flat ~100% transmission windows, T_1 and T_2, and two mirrors (M_1, M_2) of reflectivity R_1 and R_2. At the boundary conditions, the right surface of mirror M_1 becomes boundary 1 and the left surface of mirror M_2 becomes boundary 2. The laser light within the resonator is split into two components, $I^+(x, t, \lambda)$ propagating in the positive x direction and $I^-(x, t, \lambda)$ propagation in the opposite direction. $I^{\pm}(x, t, \lambda)$ is the photon spectral intensity, i.e., the photon flux per unit wavelength λ. The total laser spectral intensity $I(x, t, \lambda)$ at any point within the resonator is

$$I(x, t, \lambda) = I^+(x, t, \lambda) + I^-(x, t, \lambda). \tag{7}$$

In the treatment of the rate equations all variations in $I^{\pm}(x, t, \lambda)$, and in the molecular populations normal to the laser axis, are assumed

Table 2

Dye Parameters

		Rh6G	LD490
Stimulated emission cross section	$\sigma_e(cm^2)$	1.07×10^{-16}	?
Triplet-triplet absorption cross section	$\sigma^t(cm^2)$	5.63×10^{-18}	?
S1→S2 absorption cross section	$\sigma^1(cm^2)$	1.5×10^{-19}	?
G→S1/S2 absorption cross section	$\sigma^0(cm^2)$	4.01×10^{-16}	8.74×10^{-17}
Fluorescence lifetime	$\tau_f(sec)$	5.5×10^{-9}	$\sim 5 \times 10^{-9}$
Intersystem crossing rate constant	$K_t(sec^{-1})$	18×10^6	?
Molar decadic extinction coefficient	$\varepsilon(litre\ mole^{-1}\ cm^{-1})$	10.5×10^4	2.3×10^4
Fluorescence quantum yield	Q_f	0.901	0.72

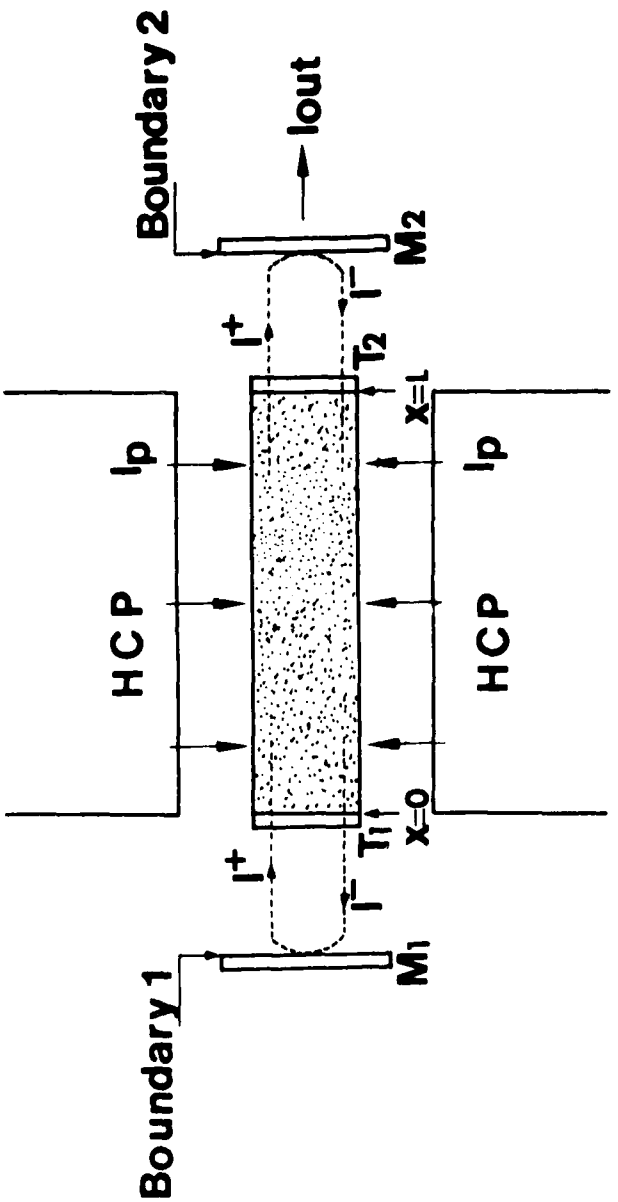

FIGURE 3. ELEMENTARY LASER SCHEMATIC OF HCP. THE BROKEN LINES REPRESENT THE CIRCULATING LASER EMISSION CONTAINED WITHIN THE RESONATOR.

to be averaged out.

The rate equations for the molecular population density N_1 in the first excited state S1 is

$$\frac{\partial N_1(x,t)}{\partial t} = W(t)\ N_0(x,t) - \frac{N_1(x,t)}{\tau_f} - N_1(x,t) \int \sigma_e(\lambda)\ I(x,t,\lambda)\ d\lambda$$

$$+ N_0(x,t) \int \sigma^0(\lambda)\ I(x,t,\lambda)\ d\lambda \qquad (8)$$

where W(t) is the pump rate (s^{-1}). The intersystem crossing rate K_t is included in the fluorescence lifetime τ_f. In equation (8), depopulation of the S1 state due to the excited state absorption at the pump or laser wavelengths is neglected due to the short duration of the S2→S1 transition as compared to τ_f. $N_1(x,t)/\tau_f$ is a spontaneous emission, and this term decreases the population density N_1. The stimulated emission is represented by $N_1(x,t) \cdot \int \sigma_e(\lambda)\ I(x,t,\lambda)\ d\lambda$. The stimulated emission also leads to the depopulation of N_1 for the S1 state. Consequently, both the stimulated emission and the spontaneous emission lead to laser action. Therefore, the total laser spectral intensity, $I(x, t, \lambda)$ is increased by these two emissions. Lastly, the ground state absorption is represented by $N_0(x,t) \cdot \int \sigma^0(\lambda)\ I(x,t,\lambda)\ d\lambda$. The ground state absorption at the laser wavelength increases the population density N_1.

Higher excited triplet states also decay nonradiatively in times on the order of 10^{-11} sec or less, so that the depopulation of the T1 state due to T1→T2 absorption can be also neglected. Thus leading to the rate equation for the triplet state population density N_t as

$$\frac{\partial N_t(x,t)}{\partial t} = K_t\ N_1(x,t) - \frac{N_t(x,t)}{\tau_t} \qquad (9)$$

where $K_t N_1(x,t)$ is an increment term of N_t due to molecules crossing over from S1 to T1 by intersystem crossing. $N_t(x,t)/\tau_t$ represents a phosphorescence which is the radiative transition form T1→G, therefore, the phosphorescence decreases the triplet state population density N_t.

The total molecular density N is assumed to be constant and given by

$$N = N_0(x,t) + N_1(x,t) + N_t(x,t) \quad . \tag{10}$$

The equation for the photon spectral intensity inside the active medium is given by

$$\frac{n}{c}\frac{\partial I^{\pm}(x,t,\lambda)}{\partial t} \pm \frac{\partial I^{\pm}(x,t,\lambda)}{\partial x} = I^{\pm}(x,t,\lambda)\{(\sigma_e(\lambda)-\sigma^1(\lambda))N_1(x,t)-\sigma^0(\lambda)N_0(x,t) - \sigma^t(\lambda)N_t(x,t)\}+b^{\pm}(x)\frac{N_1(x,t)}{\tau_f}E(\lambda)$$

$$= I^{\pm}(x,t,\lambda)g(x,t,\lambda)+b^{\pm}(x)\frac{N_1(x,t)}{\tau_f}E(\lambda) \tag{11}$$

where $g(x,t,\lambda)$ is the gain coefficient including time and space dependence. $b^{\pm}(x)$ is a geometrical factor which takes into account the fraction of spontaneous emission going into the active volume. For transverse pumping, the pump intensity I_p is assumed to be constant with respect to x, and reduction of I_p transverse to the resonator axis (i.e., into the active medium) due to the absorption is neglected.

For the simple dye laser configuration of Figure 3, the relations are

$$I^{+}(0,\ t,\ \lambda) = R_1\ I^{-}(0,\ t,\ \lambda) \tag{12a}$$

$$I^{-}(L,\ t,\ \lambda) = R_2\ I^{+}(L,\ t,\ \lambda) \tag{12b}$$

where R_1 and R_2 are the reflectivities of the resonator mirrors M_1 and M_2. The instantaneous photon spectral intensities from each end of the resonator are $(1 - R_1)\ I^-(0, t, \lambda)$ and $(1 - R_2)\ I^+(L, t, \lambda)$. The total output spectral intensity is

$$I_{out}(t, \lambda) = (1 - R_1)\ I^-(0, t, \lambda) + (1 - R_2)\ I^+(L, t, \lambda) \qquad (13)$$

Using the boundary conditions for $I_{out}(t, \lambda)$, at boundary 1

$$I(0, t, \lambda) = I^+(0, t, \lambda) + I^-(0, t, \lambda) = (1 + R_1)\ I^-(0, t, \lambda). \qquad (14)$$

Therefore,

$$I^-(0, t, \lambda) = \frac{I(0, t, \lambda)}{(1 + R_1)} \qquad (15)$$

At boundary 2

$$I(L, t, \lambda) = I^+(L, t, \lambda) + I^-(L, t, \lambda) = (1 + R_2)\ I^+(L, t, \lambda). \qquad (16)$$

Therefore,

$$I^+(L, t, \lambda) = \frac{I(L, t, \lambda)}{(1 + R_2)} \qquad (17)$$

The equation (13) becomes

$$I_{out}(t, \lambda) = \frac{(1 - R_2)}{(1 + R_1)}\ I(0, t, \lambda) + \frac{(1 - R_2)}{(1 + R_2)}\ I(L, t, \lambda) \qquad (18)$$

In this experiment, the reflectivity of mirror M_1 was >99%, therefore $R_1 \sim 1$. Then equation (18) becomes

$$I_{out}(t, \lambda) \sim \frac{(1 - R_2)}{(1 + R_2)}\ I(L, t, \lambda) \qquad (19)$$

For threshold, the gain per unit length should be equal to or greater than the loss per unit length. This relation is given by

$$G^2(\lambda)\ R_1R_2 \simeq G^2(\lambda)\ R_2 \geq 1 \tag{20}$$

where $G(\lambda) = \exp\{\int_0^L g(x, \lambda)\ dx\}$. $G(\lambda)$ is defined as the single pass gain of the medium. After reaching threshold, the laser output is in the following form

$$I_{out} = -\ \bar{I}(t, \lambda)\ \tfrac{1}{2}\ \ln R_1R_2 \simeq -\ \bar{I}(t, \lambda)\ \tfrac{1}{2}\ \ln R_2 \tag{21}$$

where $\bar{I}(t, \lambda) = \frac{1}{L}\int_0^L I(x, t, \lambda)\ dx$ is defined as the average value (with respect to x) of the laser spectral intensity, for any time t. The ordinary photon rate equation extensively used is given as follows (Ref. 17)

$$\frac{\partial \bar{I}(t, \lambda)}{\partial t} \simeq \{2\bar{g}(t, \lambda)\ L + \ln R_2\}\ \frac{\bar{I}(t, \lambda)}{T_{rt}} \tag{22}$$

where $T_{rt} = 2\ Ln/c$ and $\bar{g}(t, \lambda) = \frac{1}{L}\int_0^L g(x, t, \lambda)\ dx$ are defined as the photon round trip transit time and the averaged value of gain (with respect to x) for any time t, respectively. n is the refractive index of the dye solution and c is the speed of light.

CHAPTER III

Experimental Results and Discussion

A. Experimental Arrangement and Electrical System

Figure 4 shows the experimental arrangement of a dye laser system with an HCP array. As shown in the figure, seven brass electrode disks, separated by six insulators, are connected in series with resistive voltage dividers. The dotted curves represent the final positions of the current sheets which produce the array of plasma rings. The plasma rings emit intense radiation over a wide range of the spectrum. The intense light emitted excites the active medium of the dye laser system and produces a high power laser. The dye was circulated by a micropump which had a 3-micrometer filter inside. This filter was inserted in order to minimize the scattering of laser emission by impurities. For best filtering, a 0.4 ~ 0.5 micrometer filter should be chosen, but in this experiment, the 3-micrometer filter was used and it was found to be satisfactory. The total amount of dye was 2 litre. A stainless steel can was used as the dye reservoir. The dye circulating system was made of stainless steel, teflon, and glass which were not chemically reactive in the methylalcohol solution of dye. The dye circulating method has normally been selected to minimize the dye degradation and the loss due to absorption by the accumulated triplet state.

M_1 and M_2 are the resonator mirrors. M_1 is a flat mirror with >99% reflectivity. M_2 is an output concave mirror which has 2-meter curvature. Several output mirrors with different reflectivities were used. These flat-concave mirror combination was chosen to satisfy the stability

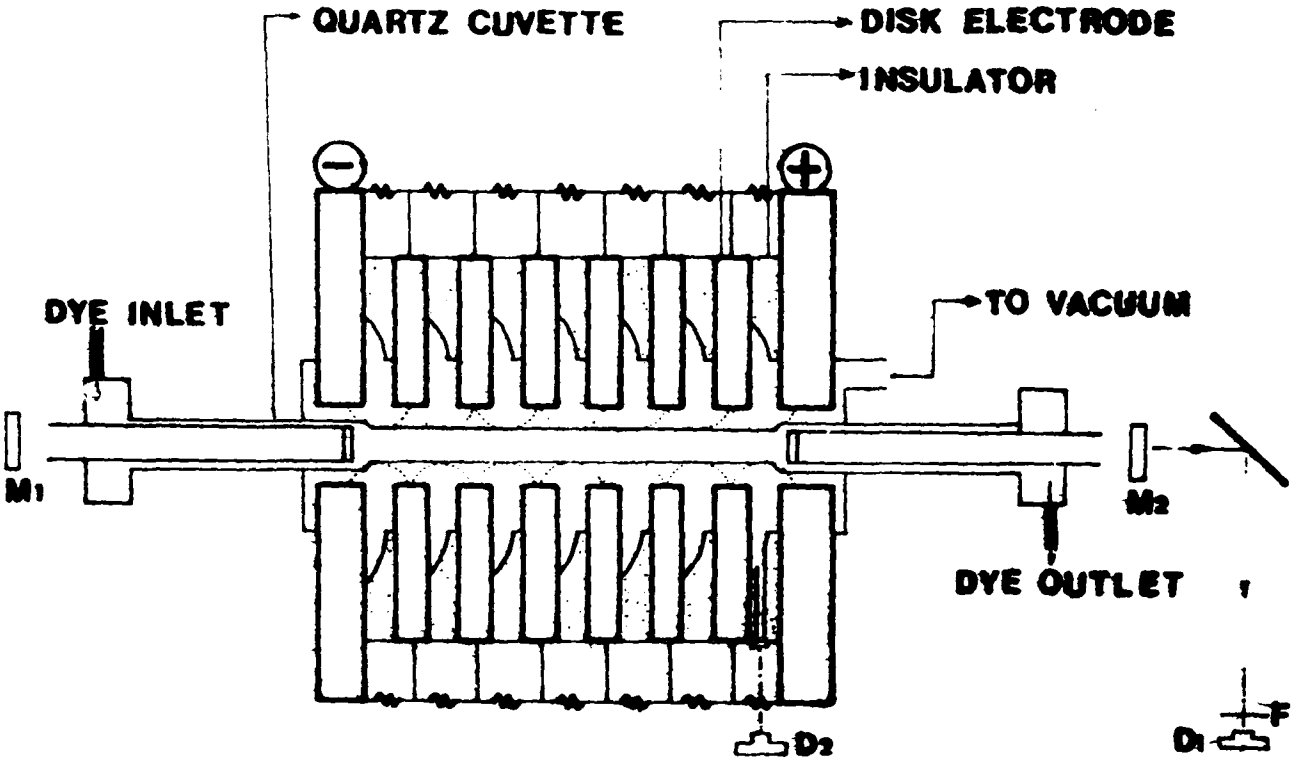

IGURE 4. EXPERIMENTAL ARRANGEMENT OF BLUE-GREEN DYE LASER PUMPED BY HCP.

condition for an optical cavity. The stability condition for the optical cavity is

$$0 < g_1 \cdot g_2 < 1 , \tag{23}$$

where g_1 and g_2 are the dimentionless quantities defined as

$$g_1 = 1 - \frac{L}{r_1}$$

$$g_2 = 1 - \frac{L}{r_2}$$

and r_1 and r_2 are the mirror radii of curvature and L is the length of the laser resonator. The calculated values of g_1 and g_2 for the HCP laser system was 1 and 0.83, respectively. Therefore, $g_1 \cdot g_2$ was 0.83 which satisfies the stability condition. The laser output and pumping light signal from the HCP were monitored with silicon diffused photodiodes (EG&G, SGD-040A), D_1 and D_2. The spectral responsivity at the wavelength of 590 nm, i.e., rodamine 6G lasing wavelength, was 0.3 A/W, and at 500 nm, i.e., LD490 lasing wavelength, was 0.25 A/W. Several neutral density filters, F, were positioned in order to protect the detector from over powering.

The dye cuvette was made of quartz or pyrex glass tubing which had a 52-mm overall length. Two different diameter glass tubes were connected to complete the dye cuvette. The large diameter for both was 13 mm and the small diameter was 8 mm or 3.5 mm. The puprose of this geometry was two fold. The first aim was to reduce the effect of the unpumped length of the active medium which causes the shift of the laser peak wavelength to longer wavelengths due to ground state absorption.

The second one was to pump the laser active medium uniformly over the whole gain length of the dye cuvette. For these purposes, a long stainless steel tube attached with a small quartz window on its end was inserted in the larger diameter glass tube so that the active length of the dye is limited to the smaller diameter tube. Both ends of the glass tube were sealed with the stainless steel tubings and teflon O-rings.

The HCP device was evacuated to a pressure less than 2×10^{-2} Torr before it was filled with argon, helium or xenon gases.

The schematic diagram of the electrical system including the HCP is shown in Figure 5. A power supply (universal voltronics, BAL-10-70) with the maximum operational range of 50 kV, 70 mA was used for charging the capacitor bank C_1. In this circuit, two processes are coupled - a charging process and a discharging process. The major components are the main capacitor bank, C_1, and the HCP as the load. The main capacitor bank, C_1, consisted fo three 2-μF capacitors connected in parallel. The parallel connection of the main capacitor banks was made with two aluminum plates which were insulated by thin mylar sheets. Because the inductance between two electrodes is proportional to the distance between the electrodes, the two closely placed aluminum plates with almost zero distance result in near zero inductance. The measured total capacitance of C_1 was 6.01 μF as listed in Table 3. The two processes of charge and discharge are controlled with switches S_1 and S_2. The switches S_1 and S_2 were electrically operated simultaneously with another manual switch. A vacuum relay was used as S_1 which had a hold-off voltage up to 50 kV. As switch S_1, a normal relay was used. The charging resistors R_1 and R_2 were chosen to control the charging time

C1: 1.8μF (measured capacitance 2.03μF), 60kV main capacitor bank
C2: 360pF, 40kV R1: 1MΩ R2: 10MΩ
R3: 10kΩ, 2W R4: 1kΩ, 2W S1: charging switch
S2: trigger switch

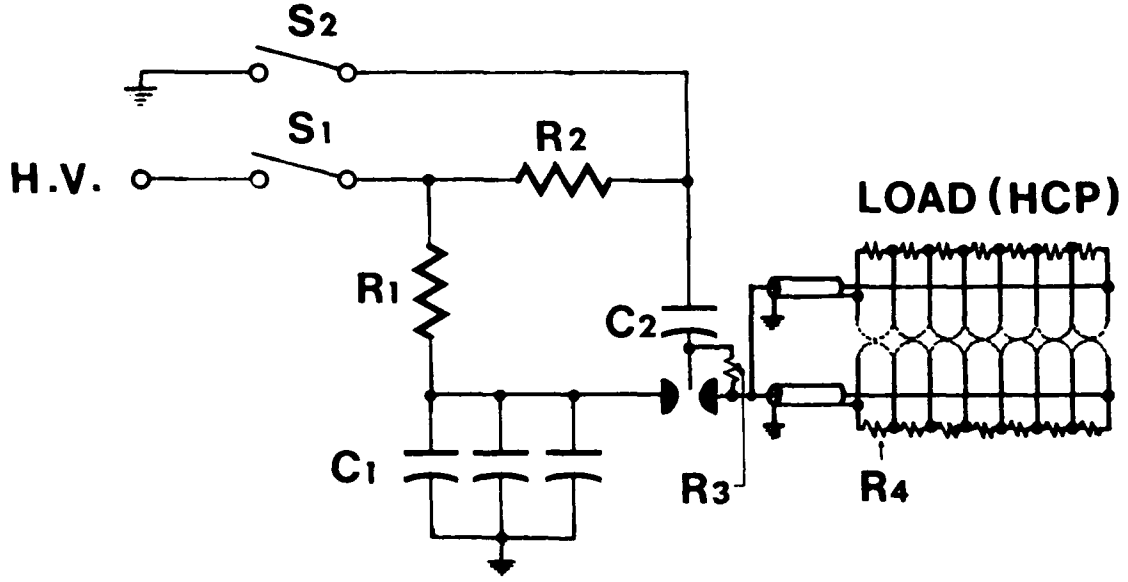

FIGURE 5. SCHEMATIC DIAGRAM OF THE ELECTRICAL SYSTEM.

Table 3

Characteristics of the Main Capacitor Bank

Number of capacitors	3
Number of switches	1
Maximum voltage	60 kV
Total Capacitance	6.09 μF
Total energy	11 kJ
Total inductance	20 nH
Inductance of one capacitor	60 nH
I_{max} on short circuit	200 kA

and to prevent over loading the power supply. By connecting resistor R_3 between the trigger capacitor, C_2, and the load, a closed circuit for C_2 was constructed. In order to minimize the inductance of the circuit, all components were connected as close as possible with coaxial cable. High voltage closed toroid type terminators were capped on the resistors R_1 and R_2 for minimizing the leakage and corona losses. The calculated value of the circuit inductance is shown in Table 4. The HCP and the main capacitor bank were separated by a spark gap while charging. When the charging process was finished, the spark gap was initiated by the voltage applied on the trigger pin which was produced by closing S_2. At the same time, S_1 was opened for disconnecting the power supply. Then the energy of the capacitor bank was transferred to the load (HCP). In this experiment, a single spark gap was used and jitter associated with multiple gaps were avoided. Because only one spark gap was employed, the circuit of S_2 connected with the same power supply and ground of the main capacitor bank, it was possible to generate the trigger voltage for the spark gap. If several spark gaps had to be chosen for the discharging process, an independent power supply might be required for triggering the gaps simultaneously. The circuit parameters were investigated by detecting the induced current signal on Rogowski coils. The period of oscillation was found to be 6 μs. Therefore the rise time was about 1.5 μs and the ringing frequency was 167 kHz. The ringing frequency of an RLC circuit is calculated as

$$f = \frac{1}{2\pi}\sqrt{\frac{1}{L_t C} - \frac{R^2}{4L_t^2}} \qquad (24)$$

TABLE 4

Inductance of System

Total inductance L_t^*	149 nH
Inductance of capacitor bank L_c	20 nH
Inductance of coaxial cable L_w	47.09 nH
Inductance of HCP L_h	18.6 nH
Others (Miscellaneous) L_m	63.31 nH

$^*L_t = L_c + L_w + L_h + L_m$

where f = ringing frequency (hertz),

C = capacitance (farads),

L_t = inductance (henries), and

R = resistance (ohms).

The HCP system used had an under-damped circuit or

$$\frac{1}{L_t C} >> \frac{R^2}{4L_t^2}$$

Therefore, equation (24) can be reduced to

$$f = \frac{1}{2\pi\sqrt{L_t C}} \tag{25}$$

From equation (25), the total inductance of the system was calculated by measuring the frequency f and the capacitance C. The expression for resistance of the circuit is

$$R = 2\sqrt{\frac{L_t}{C}} \tag{26}$$

The instantaneous value of current in an oscillatory RLC circuit is calculated as

$$i = 2\pi fCV \cdot \exp\left(-\frac{R \cdot t}{2L_t}\right) \cdot \sin 2\pi ft \tag{27}$$

where $2\pi fCV$ = undamped peak current,

$\exp\left(-\frac{R \cdot t}{2L_t}\right)$ = damping factor,

$\sin 2\pi ft$ = oscillatory function, and

t = time.

The peak discharge current occurs at 1/4 period of the circuit ringing frequency. At peak current the oscillatory function $\sin 2\pi ft$ is unity,

and the expression for peak current is

$$I_m = 2\pi fCV \exp\left(-\frac{R}{8L_t f}\right) \tag{28}$$

but $1/L_tC >> R^2/(4L_t^2)$, therefore equation (28) becomes

$$I_m \simeq 2\pi fCV, \tag{29a}$$

or

$$I_m \simeq V\sqrt{\frac{C}{L_t}} \tag{29b}$$

The results of these calculation for the circuit parameters are given in Table 5.

B. Laser Output Power and Energy Versus Filling Gas Pressure

The laser output energy and power dependences on filling gas pressure for argon, helium and xenon are shown in Figures 6, 7, and 8. The maximum gain of the laser medium was normally obtained at the 15 ~ 20 Torr range of the filling gas pressure. For these data, an 8.0 mm inner diameter (I.D.) quartz dye cuvette, 4.6×10^{-4} m/l dye concentration and 1.9 kJ input energy were used. The peak laser energy with xenon gas in HCP was 1.5 times more than that for argon gas. Xenon has a higher atomic number than argon and produces more photons than argon gas. The laser output with argon was also 1.5 times larger than that for helium. The atomic numbers of xenon, argon and helium are 54, 18 and 2, respectively. Although heavier gases produce more gain, use of these heavy gases normally resulted in a longer current rise time. As explained earlier,

Table 5

Circuit Parameters

Period of oscillation T	6 μs
Ringing fequency f	167 kHz
Inductance L_t	149 nH
Resistance R	0.3128 Ω
Capacitance C	6.09 μF
Peak current I_m	156.6 kA
Rise time τ	1.5 μs
Operating voltage range	0 ~ 40 kV
Operating pressure range	1 ~ 100 Torr (Ar, Xe, He)

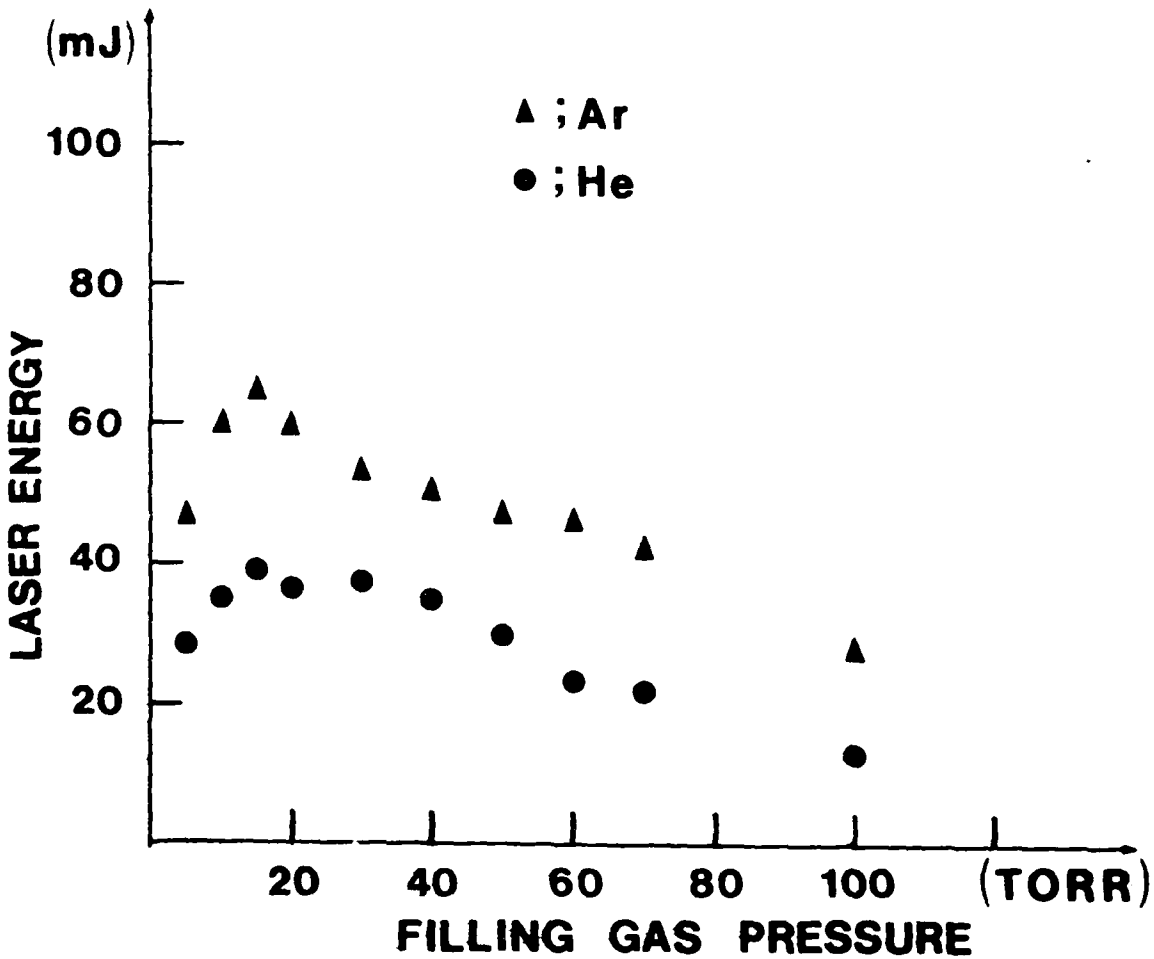

FIGURE 6. LASER OUTPUT ENERGY AS FUNCTIONS OF ARGON AND HELIUM GAS PRESSURE IN HCP. OPERATED AT AN INPUT ENERGY OF 1.9 kJ, 4.6×10^{-4} M/1 DYE CONCENTRATION, 40% TRANSMISSION MIRROR, 8.0 mm DIAMETER QUARTZ DYE CUVETTE.

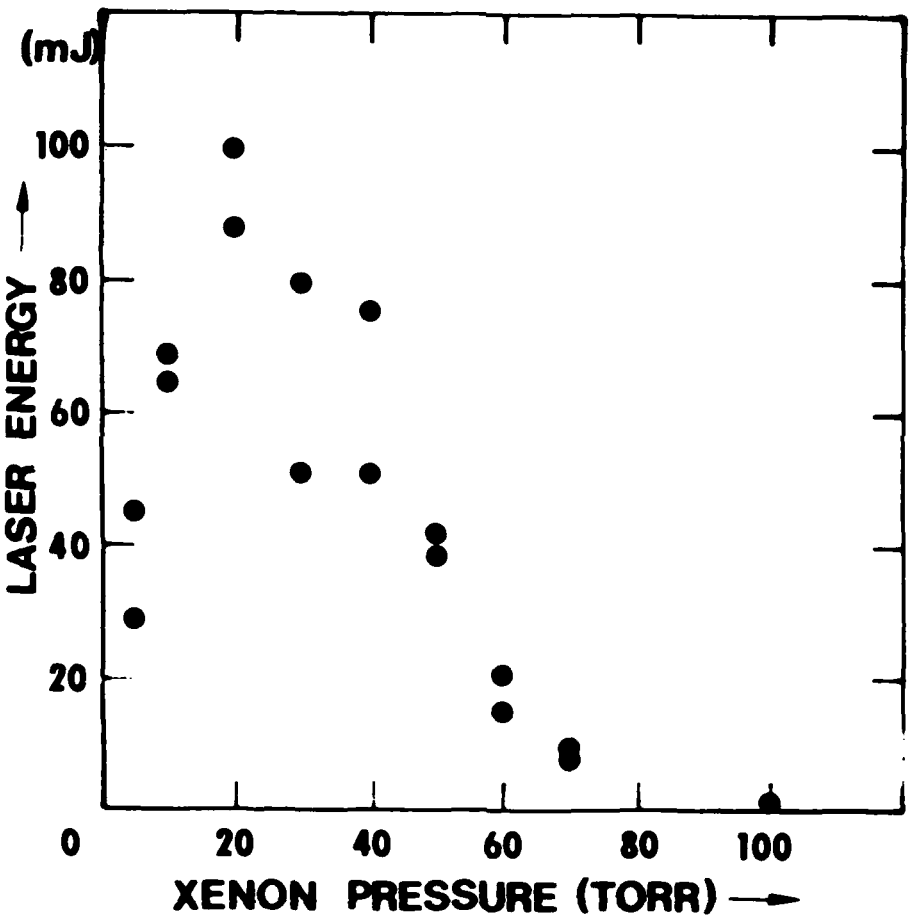

FIGURE 7. LASER OUTPUT ENERGY AS A FUNCTION OF XENON FILLING PRESSURE IN HCP. OPERATED AT AN INPUT ENERGY OF 1.9 kJ, 4.6×10^{-4} M/l DYE CONCENTRATION, 40% TRANSMISSION MIRROR, 8.0 mm I.D. QUARTZ DYE CUVETTE.

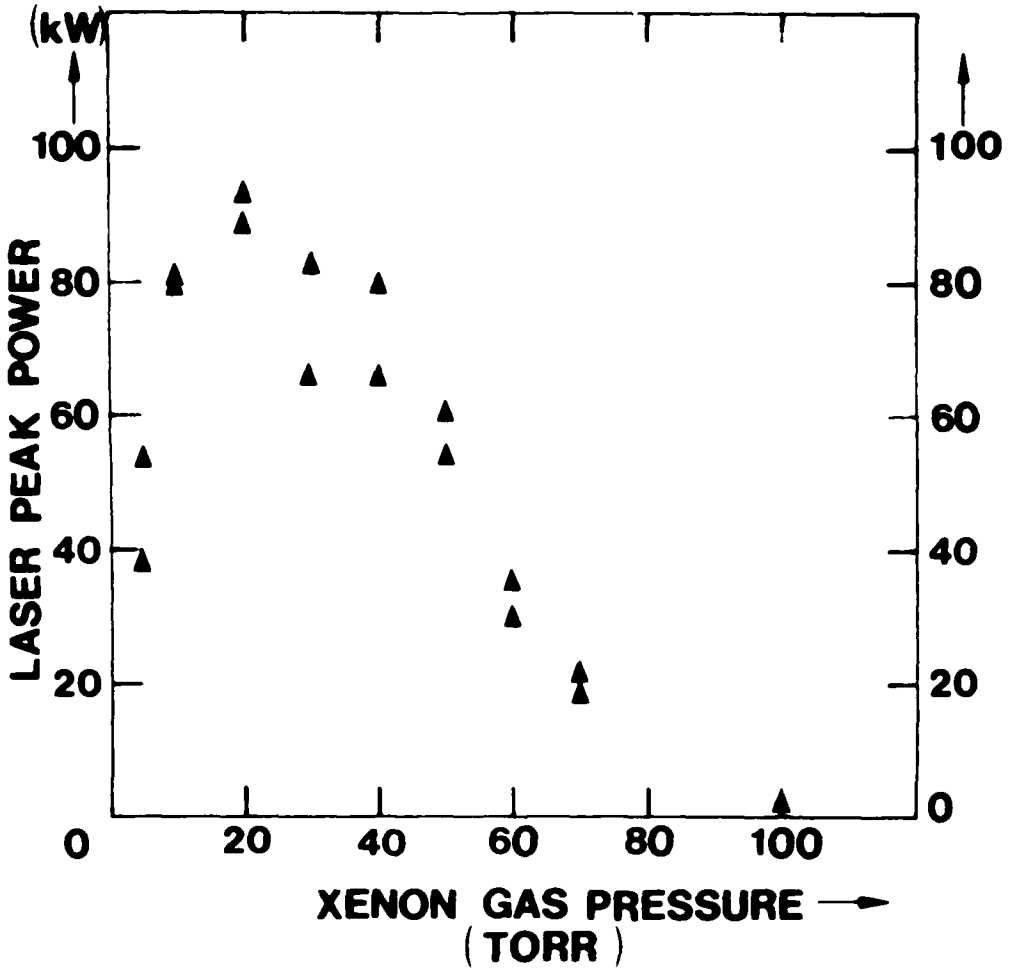

FIGURE 8. LASER OUTPUT POWER AS A FUNCTION OF XENON FILLING PRESSURE IN HCP. OPERATED AT AN INPUT ENERGY OF 1.0 kJ, 4.6×10^{-4} M/1 DYE CONCENTRATION, 40% TRANSMISSION MIRROR, 8.0 mm DIAMETER QUARTZ DYE CURVETTE.

however, the rise time strongly affected by the circuit impedance. Therefore high-voltage capacitor banks (capacitance = 6μf) were installed for this experiment and the rise time of the current, which was about 1.5 μs, did not show significant differences for different atomic weight gases.

As shows in Figure 15, the spectral pumping light energy with 20 Torr of argon filling gas pressure showed good matching with the absorption band of LD490. Because of this reason, the optimum pressure was experimentally determined as 20 Torr.

From Figures 6, 7, and 8, one may recognize the slope differences and the differences of peak laser outputs. The slope of the laser output with xenon is steeper than that of argon or helium. And the laser output terminates at 100 Torr of xenon. However, the laser output will not actually be zero. The termination of the laser output was caused by the dye degradation. For the data of laser output power and energy dependence on pressure of filling gases, quartz tubes were used as a dye cuvette. The quartz allows the UV light to transmit and damage the dye. The life time of dye, as a laser active medium, is a function of the light energy of the pumping source. The upper limit of half life can be calculated by using the following equation (Ref. 20):

$$\tau_{lim} = \frac{\mu_1}{2\mu_2} \ (J1^{-1}) \tag{30}$$

the μ's are constant for a given dye laser system. For LD490,

$\mu_1 x10^3 = 1.88$ and

$-\mu_2 x10^8 = 0.42 \ (J1^{-1})$.

Therefore, $\tau_{lim} = 224\ (kJl^{-1})$. This information indicates that a small dye volume and intense pumping light results in more rapid reduction of laser output or dye life time. Consequently, the data in Figures 7 and 8 are not truly a function of gas pressure only, but a function of gas pressure and dye degradation. If the laser output dependence on filling gas pressure is investigated by changing the dye solution for every shot, the slope of the laser output with xenon would be more mild. But this test was not performed because of the difficulty of changing the dye for every shot.

C. Laser Output Energy Dependence on Output Mirror Transmittance

Figure 9 shows the laser output dependence on the cavity tuning. In this case, the cavity loss is varied by the output mirror transmittance (T). The maximum output energy was obtained with a 40% T output mirror.

As explained earlier, the photon spectral intensity at the output mirror was described by Equation (19) as well as the Equation (6) for gain. Employing the boundary conditions such as $I^{+}(x = L, t, \lambda)$ and $I^{-}(x = L, t, \lambda)$ to Equation (17) yields the following equations

$$I(L, t, \lambda) = (1 + R_2)\ I^{+}(L, t, \lambda) \tag{31}$$

or

$$I(L, t, \lambda) = \frac{1+R_2}{R_2}\ I^{-}(L, t, \lambda) \tag{32}$$

Therefor, correlating Equations (19) and (32), we have

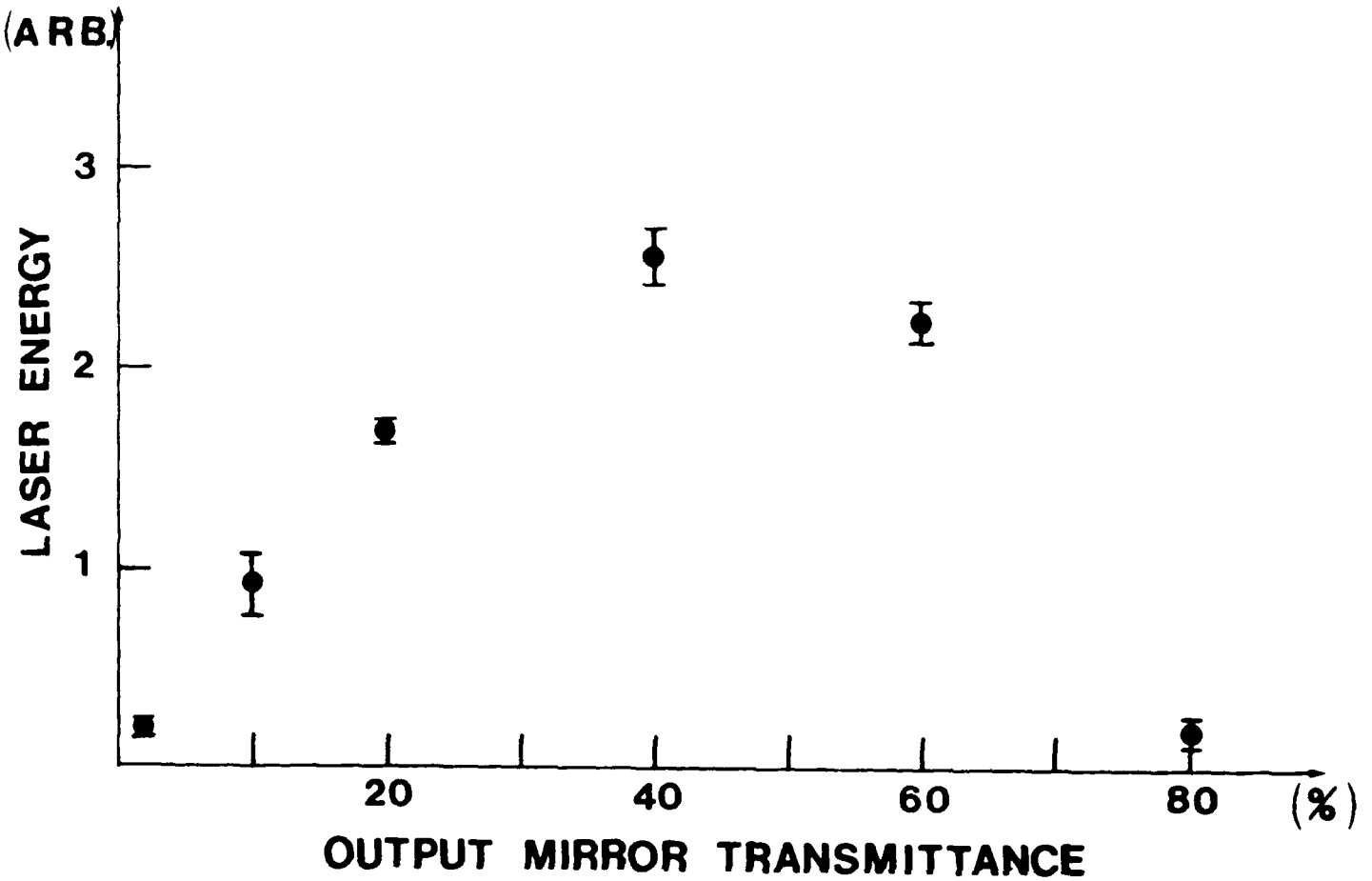

FIGURE 9. LASER OUTPUT ENERGY AS A FUNCTION OF OUTPUT MIRROR TRANSMITTANCE. OPERATED AT AN INPUT ENERGY OF 1.9 kJ, ARGON 20 TORR, 4.6×10^{-4} M/1 DYE CONCENTRATION, 8.0 mm I.D. QUARTZ DYE CUVETTE.

$$\bar{I}(L, t, \lambda) = \frac{R_2}{1-R_2} I_{out}(t, \lambda) \qquad (33)$$

The constant, $\frac{R_2}{1-R_2}$, on the right-hand side of Equation (33) represents the fractional photon loss due to the output coupling before the population inversion is reached. In Figure 9, the positive direction of the x-axis indicates the transmission increment. The transmission is increased while the reflectivity decreases. And the fractional photon loss decreases as the reflectivity R_2 of output mirror increases.

As the reflectivity R_2 decreases, the threshold energy increases due to the increased photon loss. The threshold condition was defined by Equation (20). However, as shown in Figure 9, the laser output energy increases until the transmission reaches 40%. After the threshold, the laser output can be determined by Equation (21). To interpret the experimental data shown in Figure 9 which represents the laser output as a function of mirror transmittance, Equations ((17), (20), and (21)) are employed. If the averaged value of the laser spectral intensity $\bar{I}(t, \lambda)$ becomes invariant, the laser output must be decreased by the increase in R_2 according to the correlation shown in Equation (21). However, $\bar{I}(t, \lambda)$ is varied corresponding to the gain $\bar{g}(t, \lambda)$ in the Equation (22). The pumping light intensity $I_p(t)$ is a function of time and it shows the peak value at about 2.0 μs as shown in Figure 10. The population inversion takes place over the threshold point which is determined as a function of the output mirror transmittance. Therefore, it is necessary for the threshold point to be placed at the time before the pumping light intensity, $I_p(t)$, reaches the peak point. At a certain threshold, the laser output is maximized where the peak of laser

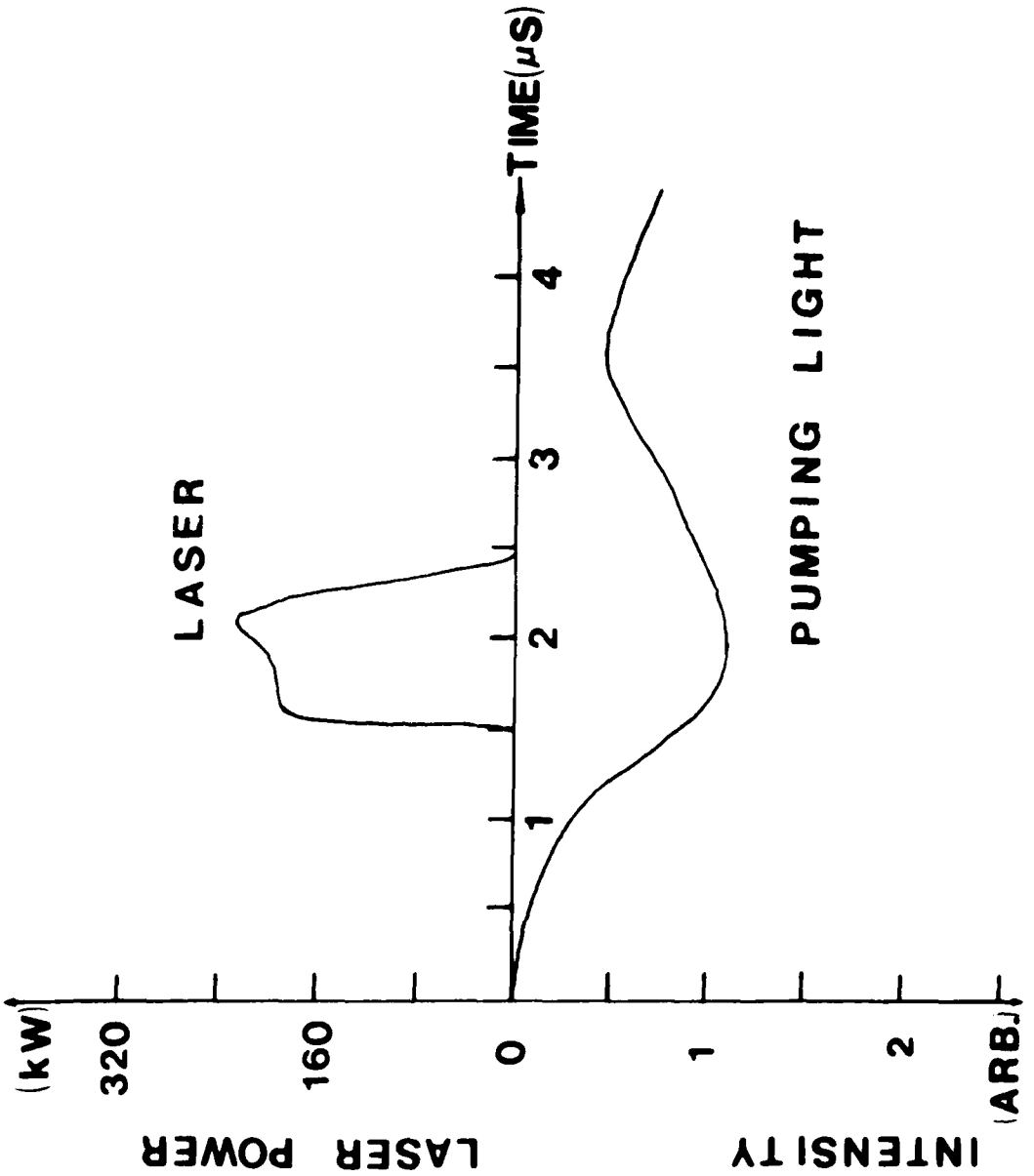

FIGURE 10. BLUE-GREEN LASER AND PUMPING LIGHT SIGNAL FROM HCP.

output approximately coincides with the peak of the pumping light intensity. Such a result is shown in Figure 10. The peak-match occured at about 2 μs. The population density N_1 at the first excited state is built up by the higher pump rate W(t) until the gain $\bar{g}(t, \lambda)$ becomes large enough so that the peak of the pumping light intensity $I_p(t)$ matches with the peak of the laser output signal which corresponds to $\bar{I}(t, \lambda)$. If the peak laser output occurs beyond the peak of pumping light intensity by means of selecting an output mirror with the lower reflectivity, the corresponding saturation time slows down to cause an increase in the triplet state population N_t. The low gain and triplet state population due mostly to the slow saturation time rapidly decrease the laser output as shown in Figure 9. The growth of the triplet state population density N_t plays a role as a significant loss factor in dye laser systems. The triplet state populations absorb the photons at the pump or laser wavelengths to build up to the excited triplet state T_n, and then decay rapidly to the state T_1. Again the phosphorescence lifetime τ_p is much longer than the fluorescence lifetime τ_f. Therefore, during laser action, the triplet state populations do not transit to the ground state G. Consequently, the increased N_t leads to the self-termination of laser action as shown in Figure 10. The light after the termination of laser action becomes useless, and the unused light attributes to the decrease in efficiency of the laser system. If the rise time of the pumping light becomes very short, in other words, the light pattern is swung to the left-hand side of time-axis in Figure 10, a significant amount of light can be accumulated for useful laser output power.

D. Laser Output Power as a Function of Number of Shots

Decreases of laser output with the repetitive shots was investigated. Figure 11 shows the experimental results for about 50 shots which began with a new dye cuvette and fresh dye solution. The laser output power gradually decreases as the number of shot increased as shown in the figure. The input energy for each shot was kept at 1.9 kJ. The optical conversion efficiency of the HCP was reported to be 0.8% (Ref. 21). Therefore, the absorbed energy was roughly 15.2 J for each shot when we assume that the total pumping light was absorbed by the laser active medium. The decrease of the laser output can be explained by two factors. The first is a dye degradation which causes absorption at the laser wavelength and consequently reduces the laser output power. The second cause may be sputtering on the dye cuvette by the brass vapor from electrodes. This vapor acts as a light attenuater. After about 50 shots, the laser output power was somewhat stable until approximately the 150th shot. This result is not shown on Figure 11. The coated dye cuvette was exchanged with a clean one after the laser output becomes stable. However, no substantial increase of the laser output was observed indicating the sputtering is not a significant factor for the decrease of the laser output as the dye degradation.

When argon and the quartz dye cuvette were used lasing was observed until about 190 shots. While with xenon and quartz cuvette only 30 shots were obtained before the laser action diminished. The xenon gas, which was the heaviest gas used in the experiment, produced more intense light than argon gas. Accordingly, the more intense light produced, the

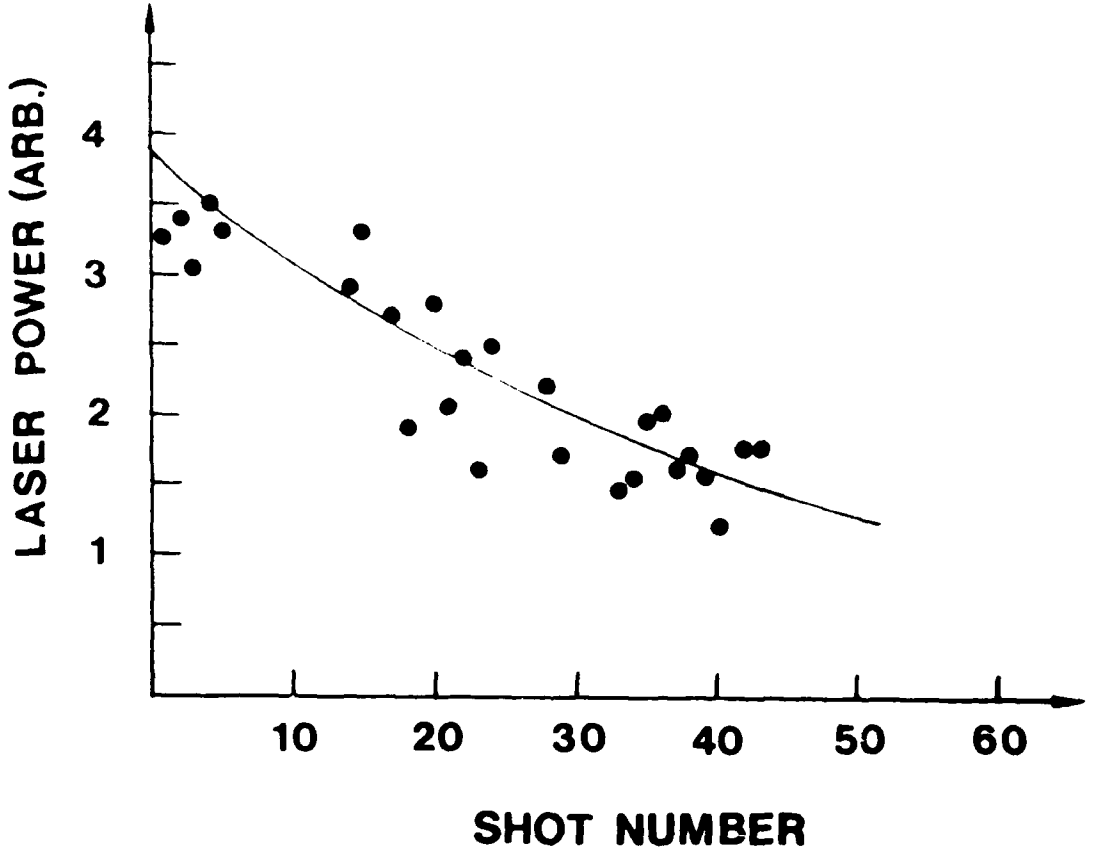

FIGURE 11. LASER OUTPUT POWER AS A FUNCTION OF NUMBER OF SHOTS.

faster the laser output decayed. With a pyrex dye cuvette, the decrease of the laser output occurred much slower than with the quartz. In this experiment, the lifetime of LD490 with a pyrex tube was not pursued. It was reported that the exclusion of UV excitation energy could increase the dye stability (or lifetime) as much as 50 folds (Ref. 20). This was indeed observed in the experiment. The dye lifetime is much longer with the pyrex cuvette than with the quartz cuvette since the transmission cutoff wavelength of quartz is 190 nm while that of pyrex is 280 nm as shown in Figure 12 (Refs. 22, 23).

E. Laser Output Energy Dependence on Dye Concentration

Figure 13 shows data for laser output energy versus dye concentration of LD490. The operating conditions for data plotted in Figure 13 were a 2% transmission output mirror, a 3.5 mm I.D. quartz dye cuvette, 20 Torr filling gas pressure of argon and 1.9 kJ input energy at room temperature. With 4.6×10^{-4} M/l dye concentration of LD490, the laser achieved the peak value of output power. For a commercially available flashlamp, 2×10^{-4} M/l dye concentration of LD490 is normally regarded as the best value of the concentration (Ref. 24).

The laser output power is in general functions of the dye concentration and the photon flux density of a laser pumping light source. Then a correlation which links the laser pumping light intensity to the dye concentration has to be made to interpret the results shown in Figure 13. Commonly while a constant light intensity is maintained, the denser the dye concentration, the higher the laser output. However, there is a limit on the dye concentration, thereafter the laser output

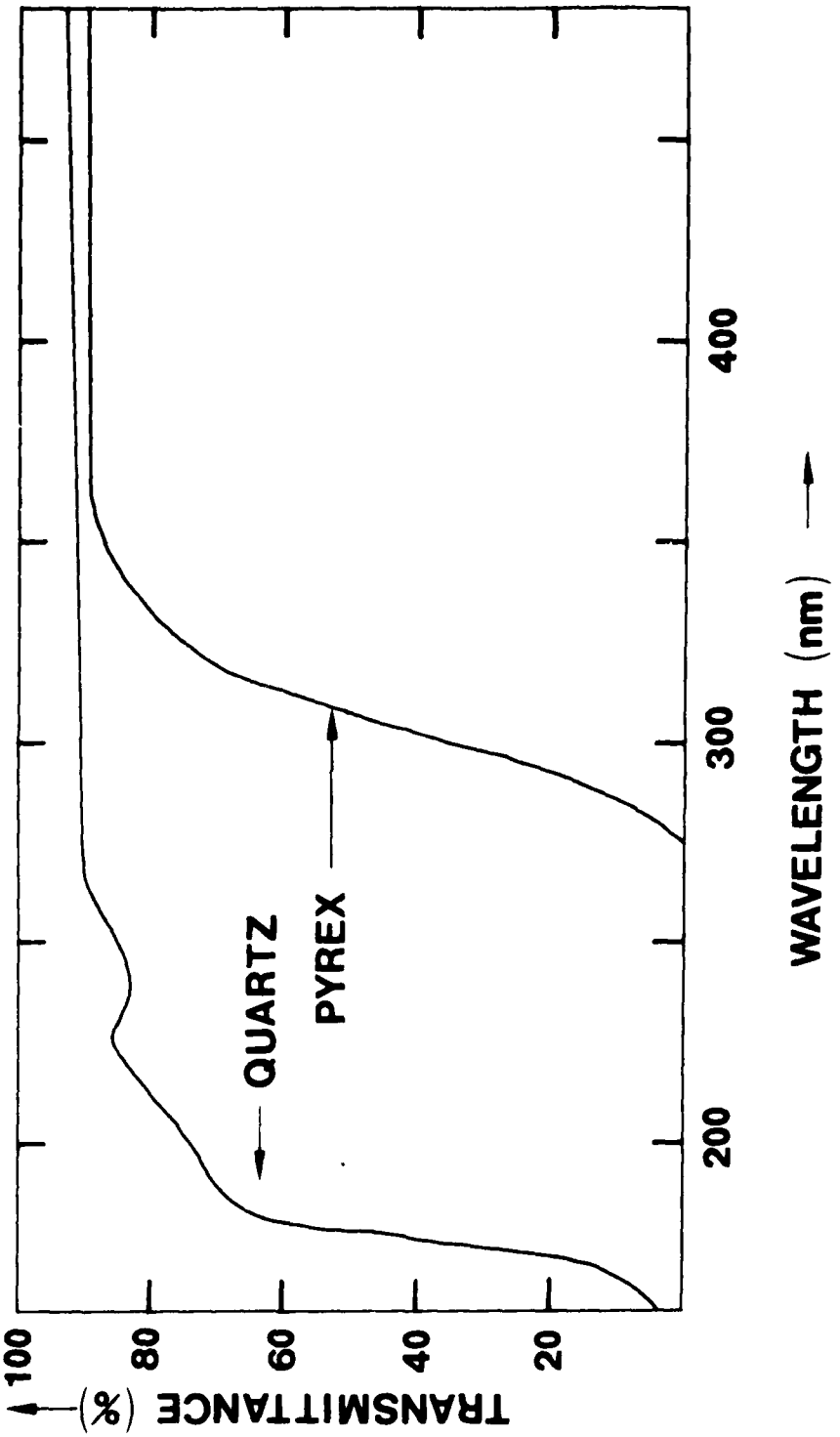

FIGURE 12. THE EXTERNAL TRANSMITTANCE OF QUARTZ AND PYREX GLASS.

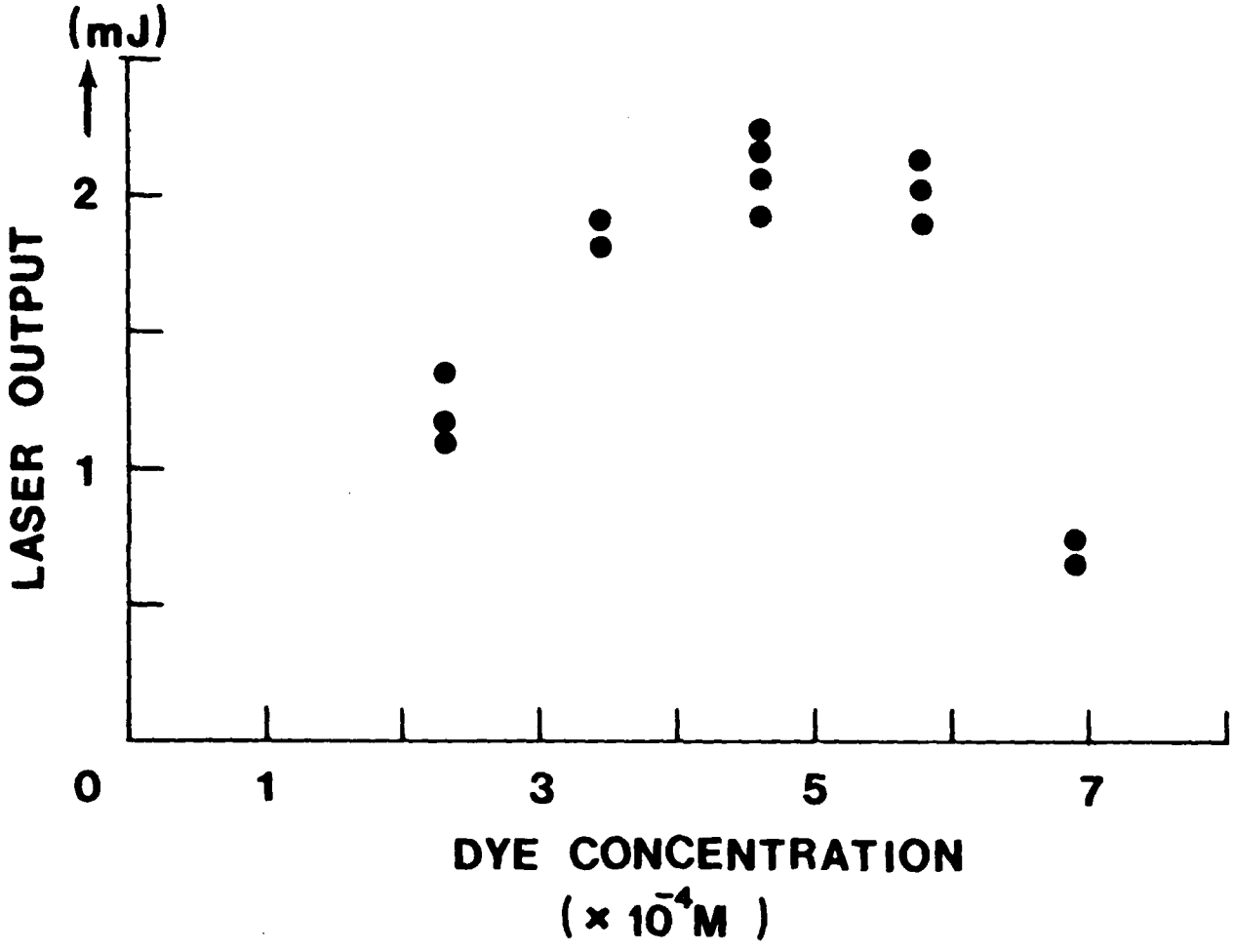

FIGURE 13. LASER OUTPUT ENERGY AS A FUNCTION OF THE DYE CONCENTRATION. OPERATED AT AN INPUT ENERGY OF 1.9 kJ, ARGON 20 TORR, 2% TRANSMISSION OUTPUT MIRROR, 3.5 mm I.D. QUARTZ DYE CUVETTE.

starts to drop significantly because the increase in opacity of the dye medium limits the penetration of light and thus localize the lasing activity of the dye on a thinly penetrated area only. On the other hand, the dye medium under the penetration depth would absorb substantial amounts of photons at the lasing wavelength during the amplification process.

The intensity of light uniformly absorbed by the laser active medium can be determined from the dye concentration for a given pumping source. Accordingly, one may expect that the pumping light intensity of HCP is much higher than that of flashlamps at the absorption band of LD490. The absorbed energy at the absorption wavelength can be expressed by the following equation

$$E_{abs}(\lambda) = E_p(\lambda)(1 - 10^{-\varepsilon(\lambda)M_c L}) \tag{34}$$

where $E_{abs}(\lambda)$ = the absorbed energy by the laser active medium at the wavelength λ (Joule)

$E_p(\lambda)$ = the pumping light energy at the wavelength λ (Joule)

$\varepsilon(\lambda)$ = the molar decadic extinction coefficient at the wavelength λ (litre cm^{-1} $mole^{-1}$)

M_c = the molar concentration of the laser active medium (mole $litre^{-1}$)

L = the length of the absorbing sample (cm).

From Equation (34), the absorbed energy will increase as the molar concentration M_c increases. The following were the actual values used in the experiment

$$\varepsilon(\lambda) = 2.1\text{x}10^{4} \text{ (litre cm}^{-1} \text{ mole}^{-1})$$

$$L = 1.75\text{x}10^{-2} \text{ (cm)}.$$

The product of these two quantities is defined as

$$a = \varepsilon(\lambda)\, L$$

$$= 3.7\text{x}10^{2} \text{ (litre mole}^{-1}).$$

Then the percent absorption, namely the ratio of the absorbed energy to the light energy becomes

$$E_{abs}(\lambda)/E_{p}(\lambda) = 1 - 10^{-aM_c} \tag{35}$$

With the parameters listed above used in the experiment, the percent absorption is 0.18 for $2.3\text{x}10^{-4}$ M/l dye concentration and 0.32 for $4.6\text{x}10^{-4}$ M/l dye concentration. The percent absorption for $4.6\text{x}10^{-4}$ M/l dye concentration is 1.8 times bigger than that of $2.3\text{x}10^{-4}$ M/l dye concentration. The laser output energy for $4.6\text{x}10^{-4}$ M/l was ~2.13 mJ and for $2.3\text{x}10^{-4}$ M/l was ~1.21 mJ. Hence, the laser output energy for $4.6\text{x}10^{-4}$ M/l was 1.76 times larger. Thus, based upon the dye concentration, one can see that the ratio of laser output (see Figure 13) determined from the experiment agrees well with the ratio of percent absorptions.

Beyond the $4.6\text{x}10^{-4}$ M/l dye concentration, the laser output dramatically decreased. In this case, the decrease in laser output was due to the fact that the light energy E_p from the HCP was mostly absorbed by the dye within a thin penetration layer of the dye curvette and the

dye beyond the optical penetration depth swallowed a substantial number of photons at the laser wavelength. This phenomenon can be easily observed by burning a Polaroid film positioned in front of the output mirror. If the dye concentration is too thin, then the burned trace on the film by the laser beam will reveal that the central area of the laser beam has more brightness than the outer area. If the burned trace at the center area is darker than at the other area, it can be concluded that the dye concentration is too thick. This observation was made using Polariod Film (Type 667) in the experiment.

F. Laser Output Energy Dependence on Input Energy

Laser output energy dependence on input energy was investigated. Figure 14 shows the experimental results of the laser output dependence on input energy. The data depicted by open circles represent the laser output energy with 2.3×10^{-4} M/l dye concentration and 20 Torr of argon filling pressure using an optical arrangement which consisted of a 2% output mirror, a 3.5 mm I.D. quartz dye cuvette. The black points were obtained by replacing the 2% T mirror, 3.5 mm I.D. quartz dye cuvette and 2.3×10^{-4} M/l concentration with a 40% T mirror, a 8.0 mm I.D. pyrex dye cuvette and 4.6×10^{-4} M/l concentration, respectively. The slope efficiency of the laser output described by those open circles in Figure 14 is as small as about 0.68×10^{-4}% and the threshold is 0.3 kJ of the input energy. However, the slope efficiency for the black point data is 42×10^{-4}% which is much greater than those of the open circle data. The threshold energy is 1.38 kJ as shown in Figure 14. The laser output varies linearly as a function of the input energy. The

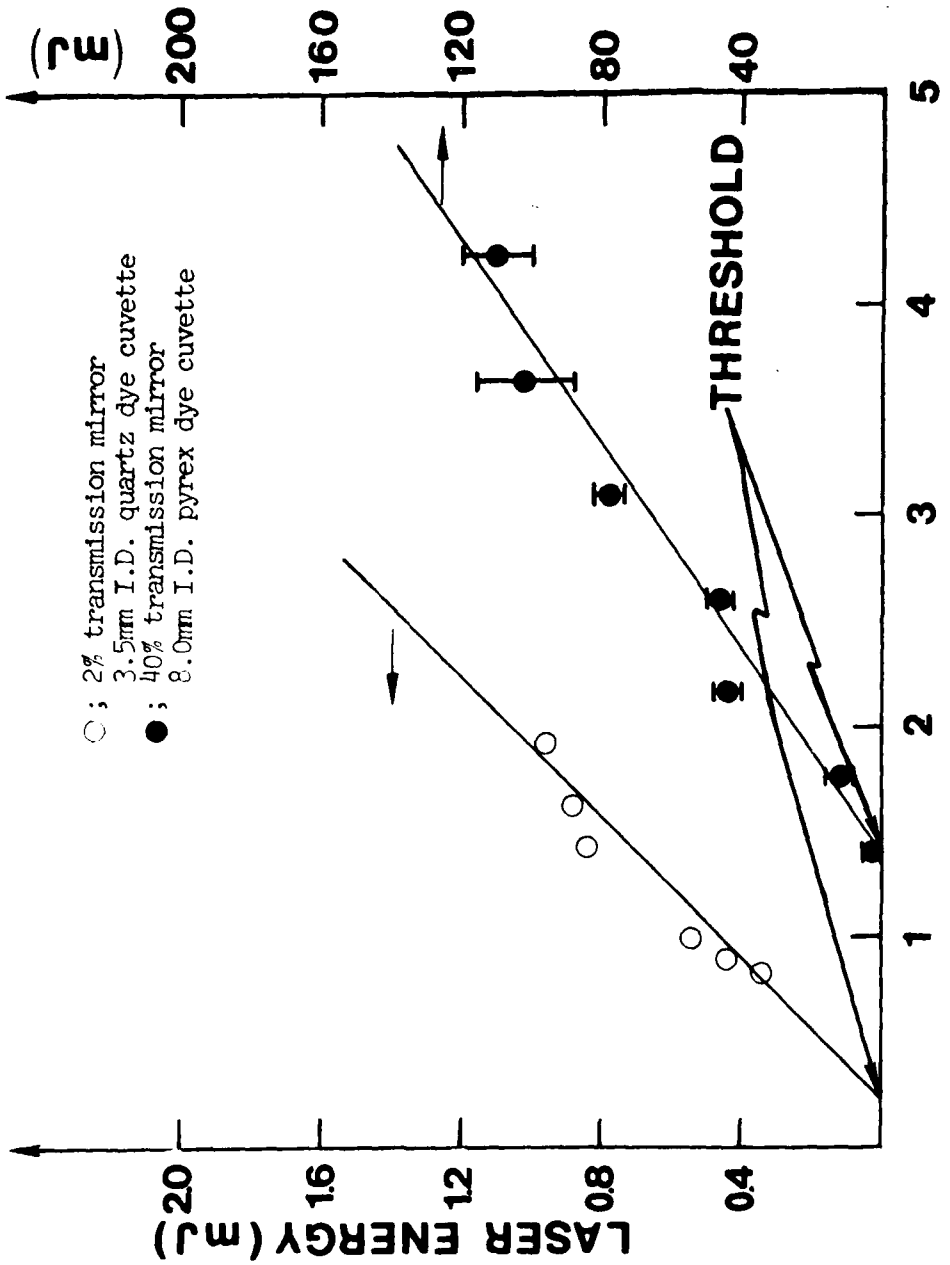

FIGURE 14. LASER OUTPUT ENERGY AS A FUNCTION OF INPUT ENERGY. OPERATED AT ARGON 20 TORR.

following equation shows the linear relationship between the input and output energies

$$E_o = BE_i \text{ (Joule)} \tag{36}$$

where E_o is a laser output energy (Joule),

B is a slope efficience (%),

E_i is an input energy (Joule).

Dividing the slope efficiency by the total volume of the laser active medium, the slope efficiency per unit volume can be defined in the following form

$$S = B/V \ (\% \ cm^{-3}) \tag{37}$$

The calculated value of S for the 2% transmission mirror and the 3.5 mm I.D. cuvette was 8.63×10^{-5} (% cm^{-3}) and the value for the 40% T mirror and the 8.0 mm I.D. dye cuvette was 101.9×10^{-5} (% cm^{-3}). From the latter case, S becomes 12 times higher than the former one. The reason why the efficiencies are so different can be explained by the laser output dependence on the output mirror transmittance. As mentioned earlier (see Figure 9), the optimum condition of laser output occurred for a 40% T output mirror. At this point, the laser active medium absorbed more energy due to the time dependence of the pumping light from the HCP and resulted in the highest gain. The laser output with the 40% T mirror was 10 times bigger than the output with a 2% T mirror. This value is in agreement with the difference for the slope efficiencies per unit volume, S.

The threshold energy difference is due to the output mirror transmit-

tance. The effects of dye concentration and volume may be resulted in a combined aspect. The optical conversion efficiency of the HCP was reported to be 0.8% (Ref. 21). Therefore the actual threshold energy for the 2% T mirror is 2.4 J and for the 40% T case it is 11.0 J. Then the threshold energy difference between two different data is 8.6 J. For many coumarin dyes, the threshold energies have been reported to be about 12 J for flashlamp pumping (Ref. 25). According to the reference, the lasing performance of many coumarin dyes was investigated using a quartz dye cell (3 mm diameter, 14 cm long) which was located in the center of a 30 cm long cavity formed by both a curved (0.5-m radius of curvature) and a plane broad-band mirror having 99% and 94±2% reflectivities, respectively. For this system, the output mirror transmittance was ~6%. Even though these investigators used a very low transmittance mirror, the threshold energy they obtained was about the same as the threshold energy of HCP laser system using a 40% T mirror. This difference indicates that the emission of the HCP source has a better spectral distribution for pumping a blue-green laser and a better coupling of the source and the dye medium.

G. Spectroscopic Analysis of the Pumping Light of HCP

The spectral energy distribution of the pumping light of HCP from 200 nm to 460 nm is shown in Figure 15. The operating conditions of the HCP are as follows. The input energy was 1.9 kJ and the fill pressure of gases (argon and xenon) was 20 Torr. An 8.0 mm I.D. quartz or pyrex glass tube was inserted along the axis of the HCP and through which the emitted light was sampled.

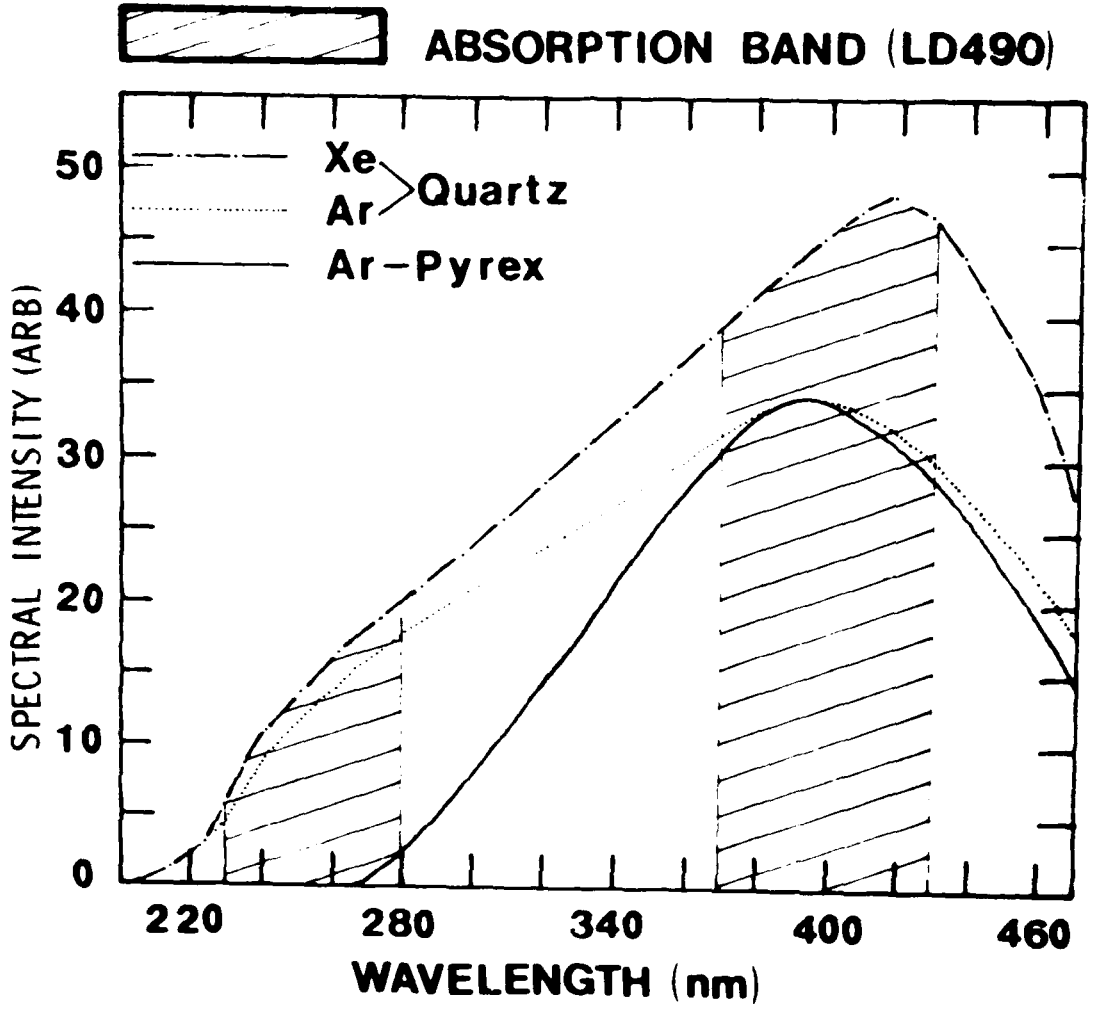

FIGURE 15. SPECTRAL ENERGY DISTRIBUTION OF HCP LIGHT FOR ARGON AND XENON GASES IN HCP WITH QUARTZ AND PYREX TUBE FROM 250 nm TO 470 nm. OPERATED AT AN INPUT ENERGY 1.9 kJ, FILLING GAS PRESSURE OF 20 TORR.

As was noticed earlier, the laser output had the maximum value at the ~20 Torr filling gas pressure. The spectral distribution of pumping light with 20 Torr gas pressure also showed that the peak wavelength of pumping light matched very well with the absorption peak wavelength.

The spectrum of the pumping light was recorded on a KODAK spectroscopic plate (type 103-F) and the plate was developed with KODAK developer D-19 for 2 minutes. This plate was positioned inside the 1.5-m McPherson spectrometer. By using a microdensitometer, the density distribution of the pumping light for both continuum and line spectrum were traced. The continuum part of the spectrum was chosen and the following relation was used for converting the optical density into the energy density deposited (i.e., exposure) (Ref. 26).

$$D = \gamma \log E \tag{38}$$

where D is a diffuse density,

E is an exposure, and

γ is a coefficient depending on development time.

The spectral response dependence of the spectrometer was not included but the spectral sensitivity of the plate from 200 nm to 460 nm was taken into account from the KODAK data book (Ref. 26).

In Figure 15, the solid curve represents the spectral distribution which was obtained using the pyrex glass tube and argon gas. The dotted line shows the distribution with quartz tube and argon gas. The dashed line was obtained with xenon gas and quartz tube. The shaded area represents an absorption band (FWHM) of LD490 which contributes to laser excitation. The peak wavelength of the spectral distribution with xenon

is 418 nm and with argon for both quartz and pyrex is 394 nm. The peaks of the spectra are matched well with the right side of the absorption band which covers from 370 nm to 430 nm. The other absorption band (FWHM) lies from 230 nm to 280 nm. From this data, one can see the integrated energy difference at the apsorption wavelength not only between filling gases, but also between pyrex and quartz tubes. The emitted light energy from xenon gas with the quartz tube at the absorption band was 1.3 times greater than that from argon gas with the same tube. Therefore, the laser output with xenon gas was 1.5 times more than that with argon filling gas for the quartz tube, as was explained in section B of this chapter.

Figure 12 shows the transmission curves of quartz and pyrex tubes for 1 mm thickness, which include surface reflection losses. The pyrex cuts off the UV portion (below 280 nm) and the quartz transmission cutoff is about 190 nm. This characteristic can also be noticed from Figure 15. The light intensity with the pyrex tube and argon terminated at about 270 nm and the light with quartz and argon terminated at ~200 nm. Because of these transmission characteristics, the UV light is cutoff by the pyrex tube before reaching the laser active medium. The UV light within the absorption band contributes to exciting the dye molecule to the higher excited state S2. This excited molecule transits to the first excited state, S1, rapidly (intersystem crossing) and increases the population density, N_1. Therefore, the UV light loss due to pyrex transmission cutoff will decrease the laser output energy. The area difference between the visible and the UV absorption band was 1.4. The resulting laser output with pyrex was reduced by 1.5 from that with

quartz. This laser output difference agrees well with the area difference of the two LD490 absorption bands.

H. Laser and Fluorescence Spectrum of LD490

Figure 16 shows the spectrometer system used for measurement of the spectral distribution of the laser beam. The components of the system indicated in Figure 16 are as follows:

M_1; A flat mirror with >99% reflection, λ_c = 490 nm, $\Delta\lambda$ = ± 60 nm, where λ_c is the center of wavelength of a mirror.

M_2; A concave mirror with 60% reflection (2 m curvature), λ_c = 500 nm, $\Delta\lambda$ = ± 60 nm.

B.S; Beam splitter

M_3; A plane mirror

D.G.; Diffused glass

L; 8.0 cm focus lense

S_1; Slit 1 (opened 10 μm)

S_2; Slit 2 (opened 70 μm)

P.M.; RCA 1P28 photomultiplier

F; Neutral density filter

P.D.; Silicon diffused p-i-n photodetector (EG&G, SGD-040A)

The laser beam coming out through the output mirror M_2 was splitted into two beams through the beam splitter (B.S). One of the splitted beams was directed into the photodetector (P.D.) and the other toward the spectrometer. The latter beam reflected by the mirror M_3 toward the diffused glass (D.G) which was used to obtain a virtual light source for the

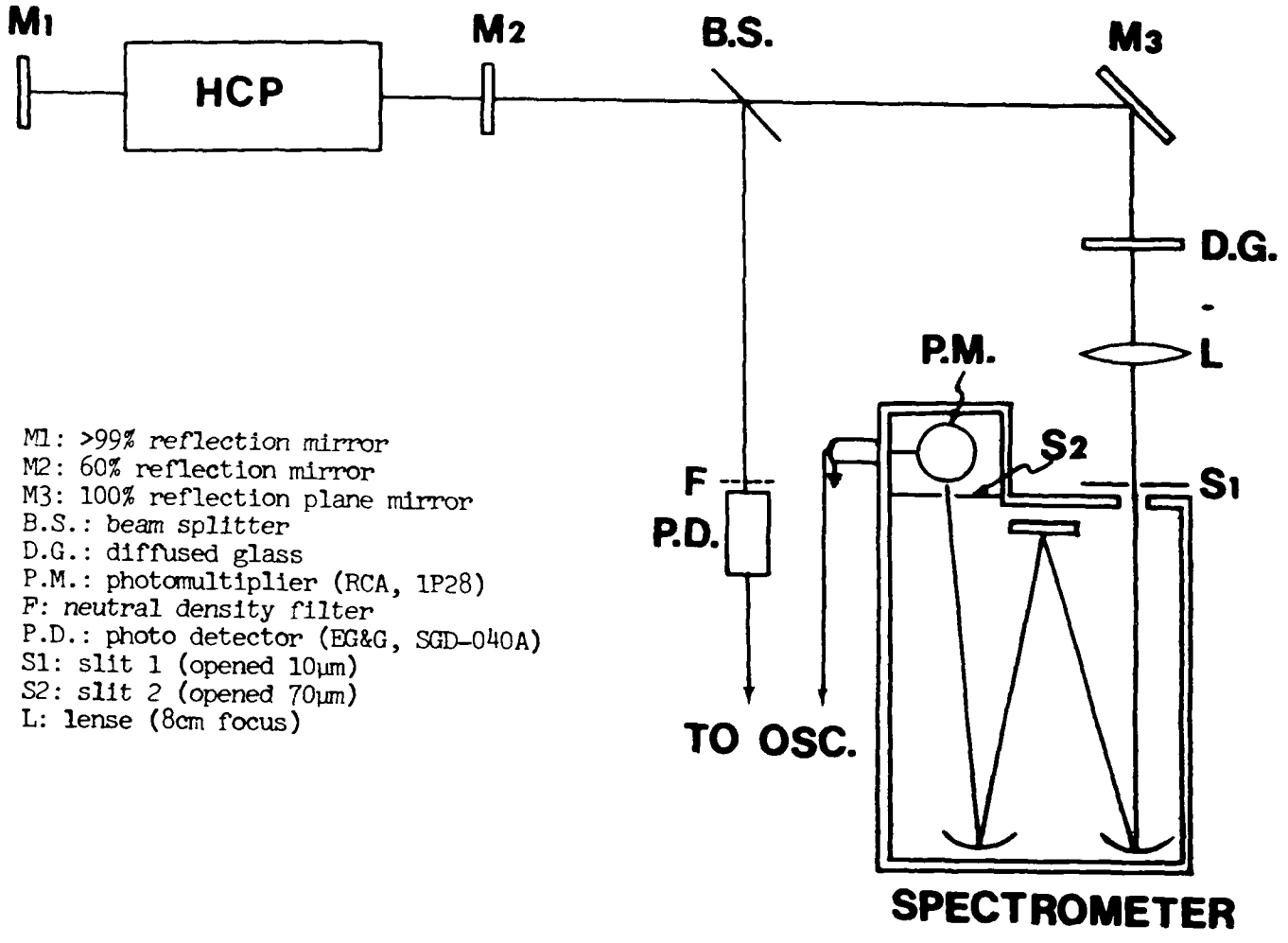

M1: >99% reflection mirror
M2: 60% reflection mirror
M3: 100% reflection plane mirror
B.S.: beam splitter
D.G.: diffused glass
P.M.: photomultiplier (RCA, 1P28)
F: neutral density filter
P.D.: photo detector (EG&G, SGD-040A)
S1: slit 1 (opened 10μm)
S2: slit 2 (opened 70μm)
L: lense (8cm focus)

FIGURE 16. SPECTROMETER SYSTEM USED TO MEASURE THE SPECTRAL DISTRIBUTION OF LASER.

spectrometer. The diffused laser beam was collected by the lense L and imaged on the slit S_1. This slit opening of 10 μm was adequate to operate the system within the linear range of the photomultiplier. The spectrum was produced at the slit S_2. The slit S_2 was kept at 70 μm which corresponded to about 1 angstrom spectral dispersion. The center-wavelengths were varied between 495 nm and 513 nm. The beam passing through the exit slit was detected by a RCA 1P28 photomultiplier for the various center wavelengths. The other laser beam, which was detected by a silicon diffused photodiode (P.D.), was used as a reference to calibrate the output signal of the photomultiplier. The filter, F, was used to attenuate the laser beam intensity to within the operating range of the photodiode. These two signals were displayed on a dual beam oscilloscope (Tektronics, Type 555) and the traces were photographed with a Polariod instant film (Type 667). A trigger signal which came from the spark gap switch was used to trigger the oscilloscope. The output signal from P.M. was relatively calibrated by using the spectral sensitivity of the P.M. supplied by the manufacturer. The equation of calibration is as follows

$$P_c(\lambda) = P_0(\lambda) \left\{1 - \frac{a}{S(\lambda_m)(\lambda_m - \lambda)}\right\} \tag{39}$$

where $P_c(\lambda)$ is the calibrated laser peak power at the wavelength λ (W).

$P_0(\lambda)$ is the measured peak power of the laser output at the wavelength λ (W).

$S(\lambda_m)$ is the photomultiplier sensitivity at the wavelength λ_m (mA W^{-1}).

a is a normalization factor (mA W^{-1} nm).

λ_m is the wavelength at the reference point (nm).

λ is the measuring wavelength (nm).

When the results from the 1.5-m McPherson spectrometer-photomultiplier system were calibrated, the spectral distribution of the laser beam of LD490 became as shown in Figure 17.

The system without the output mirror M_2, slit S_2 and photomultiplier (P.M.) was used for obtaining the fluorescence spectrom of LD490 on the KODAK safety film 5062 which was positioned in lieu of the slit S_2. The fluorescence spectrum was scanned with a microdensitometer to convert it to a density curve as shown in Figure 18. The spectrum of a mercury lamp (EG&G, Model No. 6035) was used as a wavelength reference whose lines were drawn as thick vertical lines on the x-axis in the figure. The pictures of spectral responses of laser, fluorescence and the HCP pumping light including the mercury reference lines were compared as shown in Figure 19. These were taken on high speed Polariod land film (Type 57) by positioning the film at the location of slit S_2. The operating conditions for these data shown in Figures 17, 18, and 19 were an input energy of 1.9 kJ, argon gas of 20 Torr pressure, dye concentration of 4.6×10^{-4} M/1 and a 8.0 mm I.D. pyrex dye cuvette.

From these figures we find that the laser output power had the peak value at the wavelength of about 503.5 nm and had a 4.0 nm spectral half-width. The fluorescence has the peak value at 490 nm which was not matched with the wavelength of peak laser output. The reason for mismatching between the laser output peak and the fluorescence peak wavelengths may be explained as follows. Firstly, this is due to the overlapped part of the absorption and the fluorescence spectra as compared

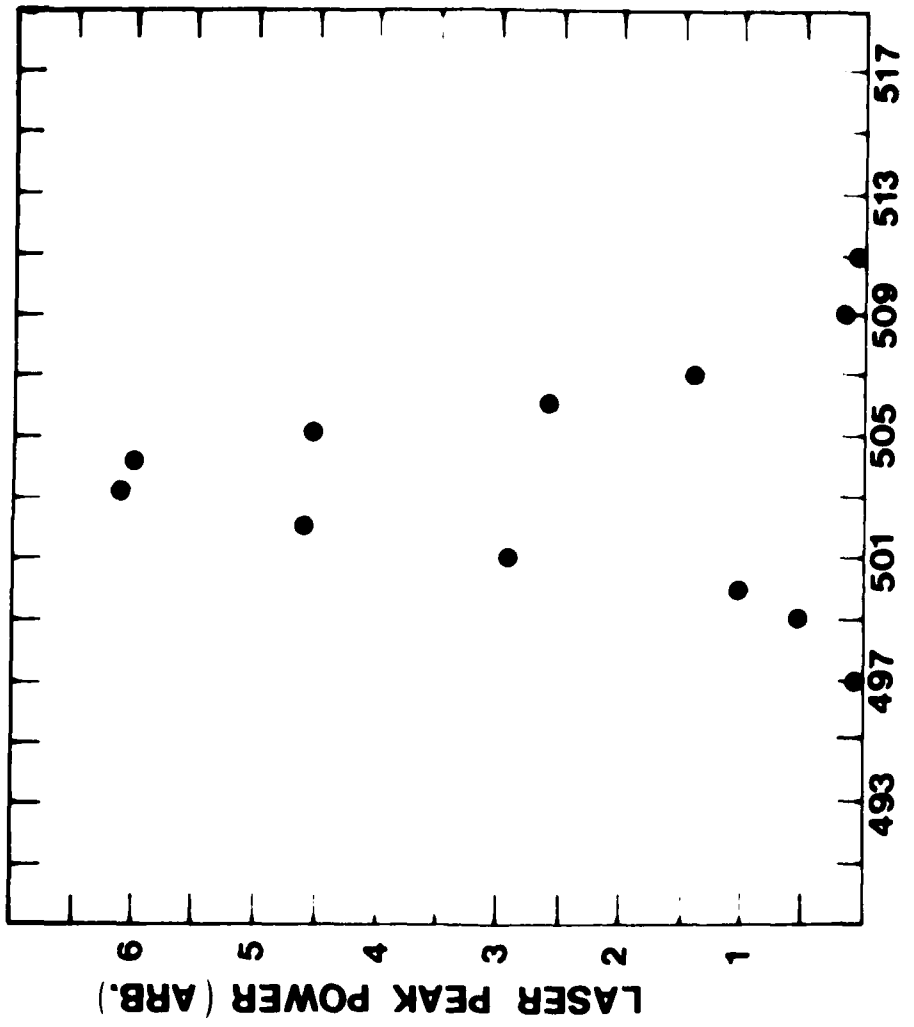

FIGURE 17. SPECTRAL RESPONSE OF LASER PEAK POWER AS A FUNCTION OF WAVELENGTH, USING A PHOTOMULTIPLIER. OPERATED AT AN INPUT ENERGY 1.9 kJ, ARGON 20 TORR, 4.6×10^{-4} M/1 DYE CONCENTRATION, 8.0 mm PYREX DYE CUVETTE.

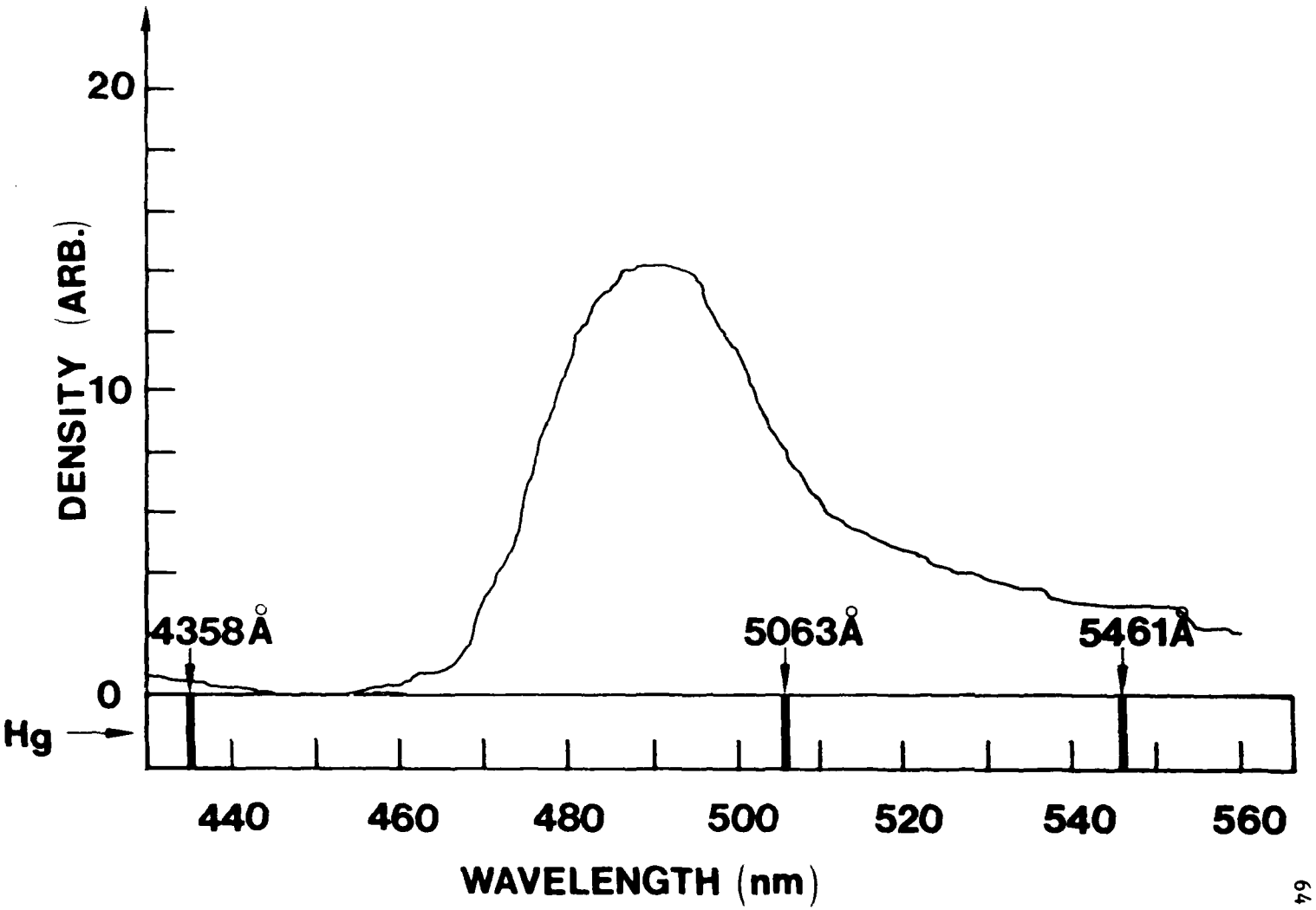

FIGURE 18. FLUORESCENCE SPECTRUM OF LD490, RECORDED ON KODAK FILM SCANNED WITH MICRODENSITOMETER. OPERATED AT AN INPUT ENERGY 1.9 kJ, ARGON 20 TORR, 4.6×10^{-4} M/1 DYE CONCENTRATION, 8.0 mm I.D. PYREX DYE CUVETTE.

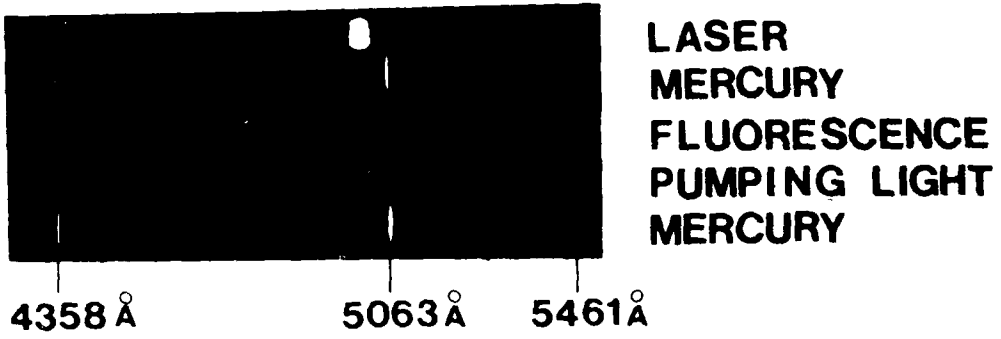

FIGURE 19. SPECTRAL RESPONSE OF LASER, FLUORESCENCE AND THE HCP PUMPING LIGHT. OPERATED AT AN INPUT ENERGY 1.9 kJ, ARGON 20 TORR, 4.6×10^{-4} M/1 DYE CONCENTRATION, 8.0 mm I.D. PYREX DYE CUVETTE.

to the results shown in Figures 18 and 20. Most of the blue-green laser dyes do not exhibit this overlapped part as claimed in Ref. 17 and more discussion about this result will be done in section I. Secondly, the mismatching is due to a part of the unpumped active medium which is caused by the configuration of the dye cell. The unpumped dye solution acts as a passive absorber at the ground state, G, and causes a shift in the laser emission peak towards longer wavelengths. But this unpumped solution does not cause the loss of the absorbed photons in the lasing process, since they repump the dye molecules and hence increase the inversion. In this experiment, the shift may be caused by the second reason.

I. Absorption Spectrum of LD490

The absorption spectrum of LD490 in the solution of methanol/water (1/1) is shown in Figure 20. The absorption spectrum has three peaks at 405 nm, 250 nm, and 225 nm. These three Gaussian type distribution curves are mainly superposed on each other and form the total absorption curve. The first absorption band with the 405 nm peak indicates the ground state absorption to the first excited singlet state S1 and has a 60 nm half-width from 370 nm to 430 nm. The second and third absorption bands with the 250 nm and 225 nm peak wavelengths represent the ground and have a 50 nm half-width from 230 nm to 280 nm, and a 15 nm half-width from 215 nm to 230 nm, respectively. The molar decadic extinction coefficients ε (litre mole^{-1} cm^{-1}) are 2.1×10^4 at the first peak, 0.8×10^4 at the second peak and 1.75×10^4 at the third peak. As discussed earlier, the second and third peak absorption bands will not contribute to the

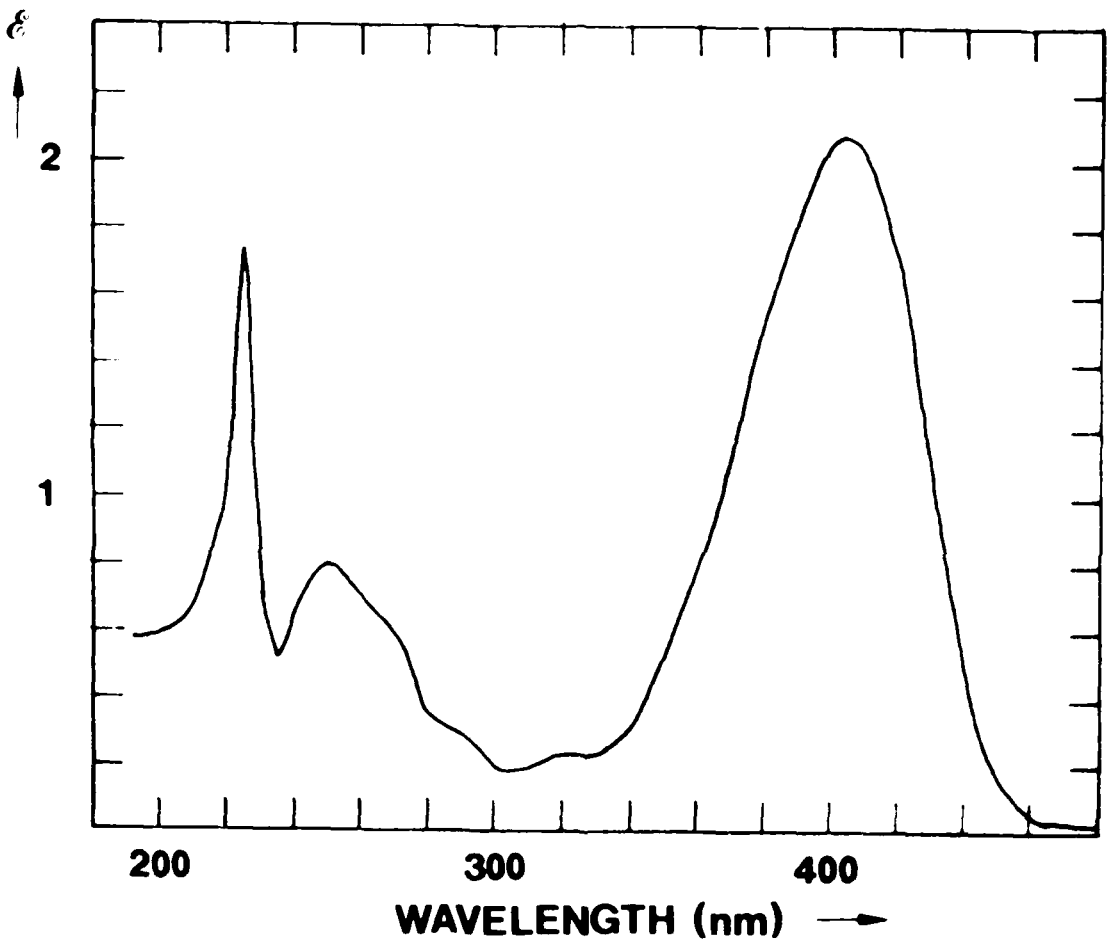

FIGURE 20. ABSORPTION SPECTRUM (LD490 IN METHANOL/WATER (1/1)).
$\varepsilon(\times 10^4$ litre mole^{-1} cm$^{-1})$; MOLAR DECADIC EXTINCTION COEFFICIENT.

laser action due largely to the transmission cut-off when a pyrex dye cuvette is used. For a quartz dye cuvette, the whole absorption band will contribute to laser action (see Figures 12 and 20). The absorbed photon energy at the first peak is about 3.06 eV and the energies of the second and third peaks are 4.96 eV and 5.51 eV.

As discussed in the earlier section, the partial overlap between the fluorescence and the absorption spectrum does not normally exist for most blue-green dye lasers. However, comparing the absorption spectrum in Figure 20 with the fluorescence spectrum in Figure 18, one can obviously recognize the area of partial overlap. The far-right of the absorption spectrum is decaying and ends at about 470 nm and for the fluorescence the far-left ends at about 460 nm. Thus, there is about a 10 nm width of the overlapping region. This area is very small compared with the non-overlapping areas. Unless there exists some unpumped solution which was explained as a second reason for a laser wavelength shift, the peak laser wavelength would be matched with the fluorescence peak. However, there was some unpumped solution that may caused the ~13 nm shift in the laser emission.

J. Laser Performance of Dyes (Rh6G, LD490) using HCP

Using LD490, the performance data of the most efficient laser output pumping by HCP was listed in Table 6. The molecular structure of LD490 is shown in Figure 21. For the data in Table 6, the laser signal shown in Figure 10 was taken. For the laser pumping in the Figure 10, 60% T output mirror was used. As an independent data, this maximum output signal is not following the result of laser output energy depen-

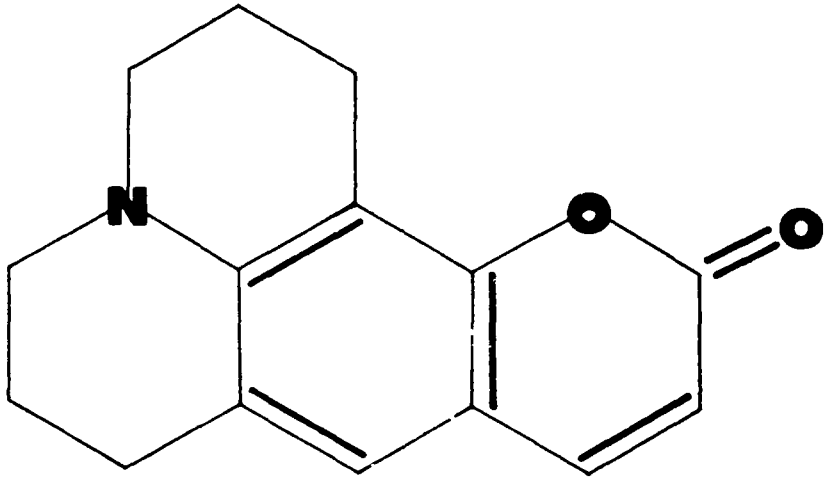

LD490

FIGURE 21. MOLECULAR STRUCTURE OF DYE LD490.

dence on output coupling shown in Figure 9 whose result has the maximum at the 40% T output mirror. From above discussion, one may recognize that the HCP laser system would have better coupling if the operating condition of the laser pumping system is properly set. The averaged power in Table 6 is obtained by considering the interval between shots which is about one minute.

In Table 7, the performance data of LD490 and Rh6G are listed. In order to compare the laser performance of these two dyes, the operating conditions are also included. The laser peak power from Rh6G is 2 kW while that from LD490 is 2.25 kW which is higher than the former. This tendency cannot be found for lasers pumped with commerical Xe flashlamps (Ref. 24). This difference is the result of the fact that the spectra of HCP at the UV wavelength is stronger than that of flashlamps which are richer in visible than UV wavelengths. As noticed earlier, the spectra of the HCP with filling gas pressure of 20 Torr shows good spectral matching with the absorption band of LD490 (see Figure 15). Consequently, the HCP laser system is suitable for pumping blue-green and UV lasers whose absorption bands lie in near and far UV wavelengths, respectively.

K. Spectral Efficiencies of Radiation for Pumping LD490

It is important to note that for a given spectral band there is an optimum temperature that maximizes the percentage of the total radiation appearing in the absorption band of the laser active medium. The purpose of this section is to study the spectral efficiencies of blackbody and bremsstrahlung radiation for pumping LD490. The spectral efficiency is

Table 6

Performance Data of LD490

Laser peak wavelength (untuned)	503.5 nm
Peak power (Max.)	230 kW
Averaged power (Max.)	3.8 mW
Pulse energy (Max.)	163 mJ
Pulse energy density (Max.)	40 mJ cm^{-3}
Pulse length (FWHM)	~1 μs
PRR	Single shot
Overall efficiency (Max.)	0.012%
Spectral width	7 nm
Concentration	4.6×10^{-4} mole $litre^{-1}$
Operating temperature	Room Temperature

Table 7

Laser Performance of Dyes (Rh6G, LD490) and the Comparison

	Rh6G	LD490
Solvent ($MeOH:H_2O$)	1:1	1:1
Dye concentration (mole litre^{-1})	1.3×10^{-4}	4.6×10^{-4}
Dye cell	Quartz	Quartz
Resonator	R_1 [illegible], R_2=98%	R_1>99%, R_2=98%
Laser peak power (kW)	[illegible]	2.25
Pulse length (FWHM) (μs)	[illegible]	~1
Laser energy (mJ)	[illegible]	2.2
Laser energy density (mJ cm^{-3}	[illegible]	2.8
Triplet quencher	[illegible]	No quencher
Dye flow unit	Recirculating	Recirculating

Table 7 (Continued)

	Rh6G	LD490
Pump cavity	HCP	HCP
Cross sectional area of the laser (cm^3)	0.096	0.096
Length of the gain medium (cm)	8.2	8.2
Length of the laser resonator (cm)	34	34
Filling pressure of argon (Torr)	20	20

defined as the ratio of the absorbed photon flux to the total incident (over all wavelengths emitted) photon flux. The primary interest of this section is the absorption spectrum of LD490 without the far UV absorption band.

The equations used for blackbody radiation are as follows (Ref. 27)

$$L_\lambda = \frac{2c^2h}{\lambda^5(e^{hc/\lambda kT} - 1)} \quad (W\ m^{-2}\ sr^{-1}\ m^{-1}) \tag{40}$$

$$M = \pi \int_0^\infty L_\lambda\ d\lambda = \sigma\ T_e^4 \quad (W\ m^{-2}) \tag{41}$$

where L_λ = spectral radiance,

M = radiant exitance,

λ = wavelength (m),

h = Plank's constant (J s),

c = velocity of light in a vacuum (m s^{-1}),

k = Boltzmann's constant (J K^{-1}), and

T_e = absolute electron temperature (K).

The Stefan-Boltzmann constant, σ, is given by

$$\sigma = \frac{2\pi^5 k^4}{15c^2h^3} = 5.6696 \times 10^{-8} \quad (W\ m^{-2}\ K^{-4})$$

The absorbed radiant photon flux density can be written as follows:

$$M_{abs} = \int_0^\infty L_\lambda (1 - 10^{-\varepsilon(\lambda) M_c L}) \, d\lambda \quad (W\ m^{-2}) \tag{42}$$

where $\varepsilon(\lambda)$ = molar decadic extinction coefficient (litre $mole^{-1}$ cm^{-1})

M_c = molar concentration of laser medium, 4.6×10^{-4} (mole litre^{-1})

L = the length of the absorbing sample, 4×10^{-3}(m).

The values of M_c and L are the actual quantities used in the experiment. Therefore, the spectral efficiency of blackbody radiation is

$$\eta_{bl} = \frac{M_{abs}}{M} \times 100 \ (\%) \tag{43}$$

The equation used for bremsstrahlung emission are as follows: (Ref. 28)

$$E_\lambda = 1.9 \times 10^{-28} N_e N_i Z^2 \bar{g} (kT_e)^{-\frac{1}{2}} \lambda^{-2} \exp(-12395/\lambda kT_e)$$
$$(W\ cm^{-3}\ angstrom^{-1}) \tag{44}$$

$$E = \int_0^\infty E_\lambda \, d\lambda = 1.5 \times 10^{-32} (kT_e)^{\frac{1}{2}} \bar{g} N_e N_i \ (W\ cm^{-3}) \tag{45}$$

where E_λ = the spectral bremsstrahlung emission per unit wavelength and unit volume

E = the total radiation power

N_e = electrons per unit volume

N_i = ions per unit volume

Z = effective nuclear charge

$\bar{g}$ = Gaunt factor

T_e = electron temperature

In Equations (44) and (45), kT_e is in eV, and λ is in angstroms. The absorbed radiation power is

$$E_{abs} = \int_0^\infty E_\lambda (1 - 10^{-\epsilon(\lambda) M_c L}) \, d\lambda \ (W\ cm^{-3}) \tag{46}$$

Therefore, the spectral efficiency of bremsstrahlung emission is

$$\eta_{br} = \frac{E_{abs}}{E} \times 100 \ (\%) \tag{47}$$

The values for calculating the spectral efficiency, η_{br}, are

$N_e = N_i = 10^{17}$ (cm^{-3}),

$Z = 1$, and

$\dot{g} = 1$.

For this computation, a VAX computer and a Tektronics 4051 Graphic System were used and the results are shown in Figures 22, 23, 24, and 25. Figure 22 shows the spectral efficiency for blackbody, η_{bl}, as a function of T. The maximum η_{bl} is 26.46% at the temperature of 9750 K (0.84 eV). Figure 23 shows the spectral radiant emittance of blackbody for two different temperatures and the absorption spectrum of LD490. At the optimum temperature (T_{opt}) of 9750 K, the peak wavelength of emittance is 297 nm which is not matched with the peak of the absorption spectrum (440 nm). In order to compare the emittance for the optimum temperature with the emittance for the temperature whose peak wavelength is matched with the peak of the absorption spectrum, Figure 23 is drawn. From this figure, one may see the reason why the peak of absorption is not matched with the peak of T_{opt} emittance. When the peak of spectral emittance matches the absorption peak, the short wavelength side of emittance shows a sharp decrease which causes a decrease of spectral efficiency. Therefore the peak of T_{opt} emittance should be shift to be shorter wavelength than the absorption peak. Consequently, the peak of T_{opt} emittance matches with the tail of the shortest wavelength of the absorption spectrum. Actually, a calculation of the temperature for maximizing the photon flux from a blackbody in the wavelength band, $\lambda_1 - \lambda_2$, has been reported

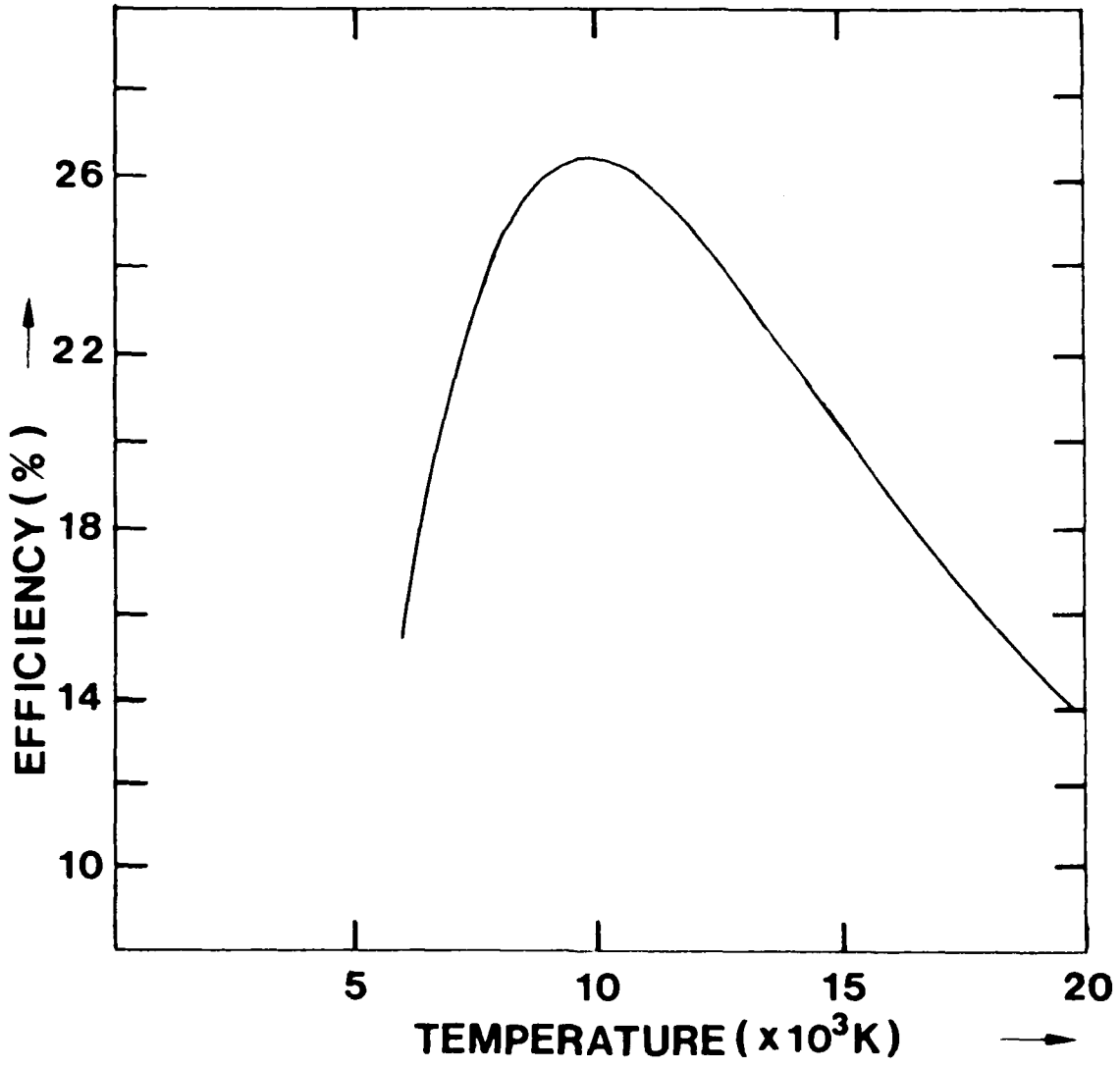

FIGURE 22. SPECTRAL EFFICIENCY OF BLACKBODY RADIATION FOR PUMPING LD490 AS A FUNCTION OF TEMPERATURE. THE ABSORPTION PROFILE OF LD490 IS TAKEN INTO ACCOUNT FOR THE EFFICIENCY CALCULATION.

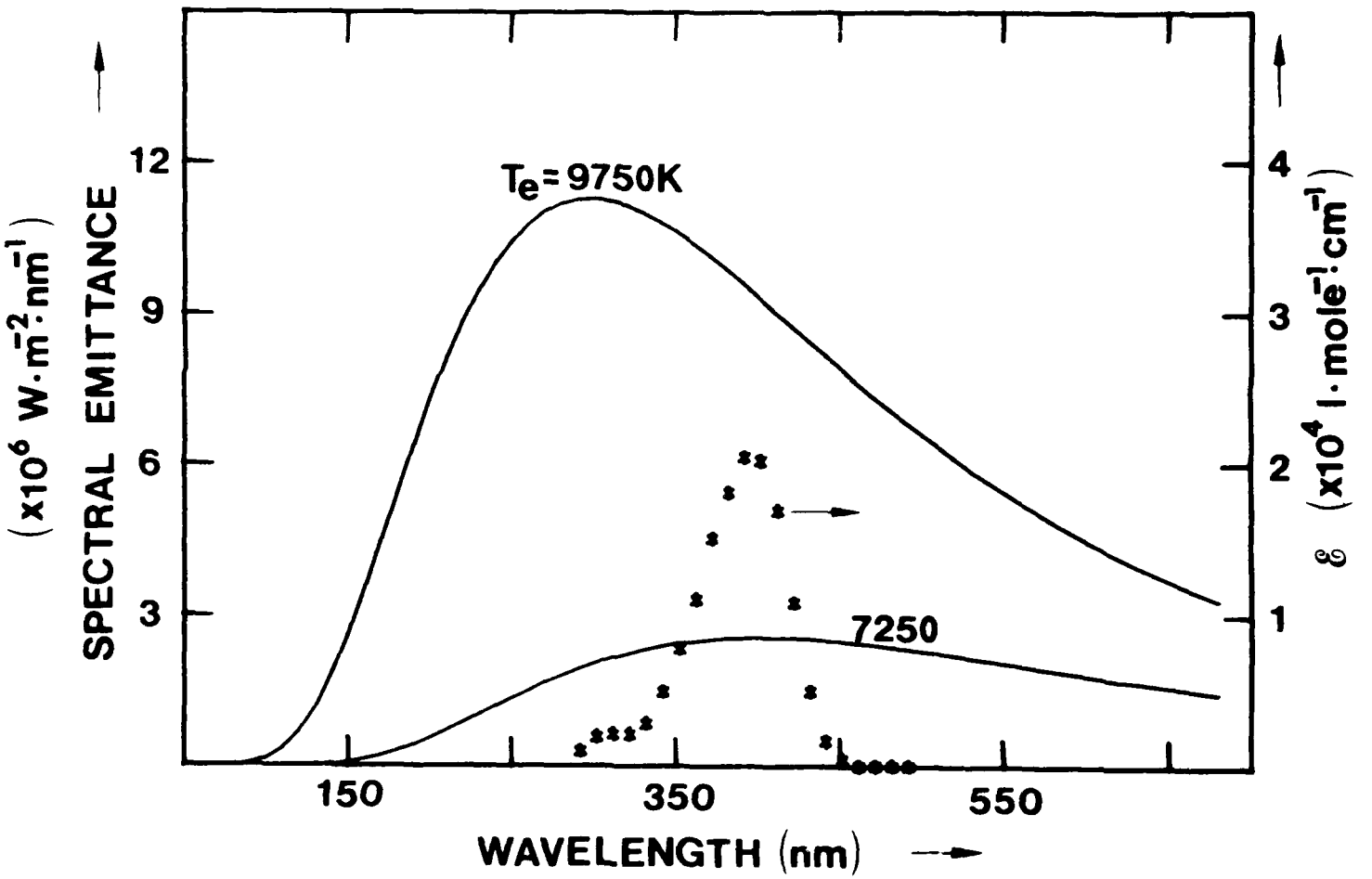

FIGURE 23. SPECTRAL RADIANT EMITTANCE OF BLACKBODY RADIATION AND ABSORPTION SPECTRUM OF LD490. 9750 K IS A T_{opt}. ϵ; MOLAR DECADIC EXTINCTION COEFFICIENT.

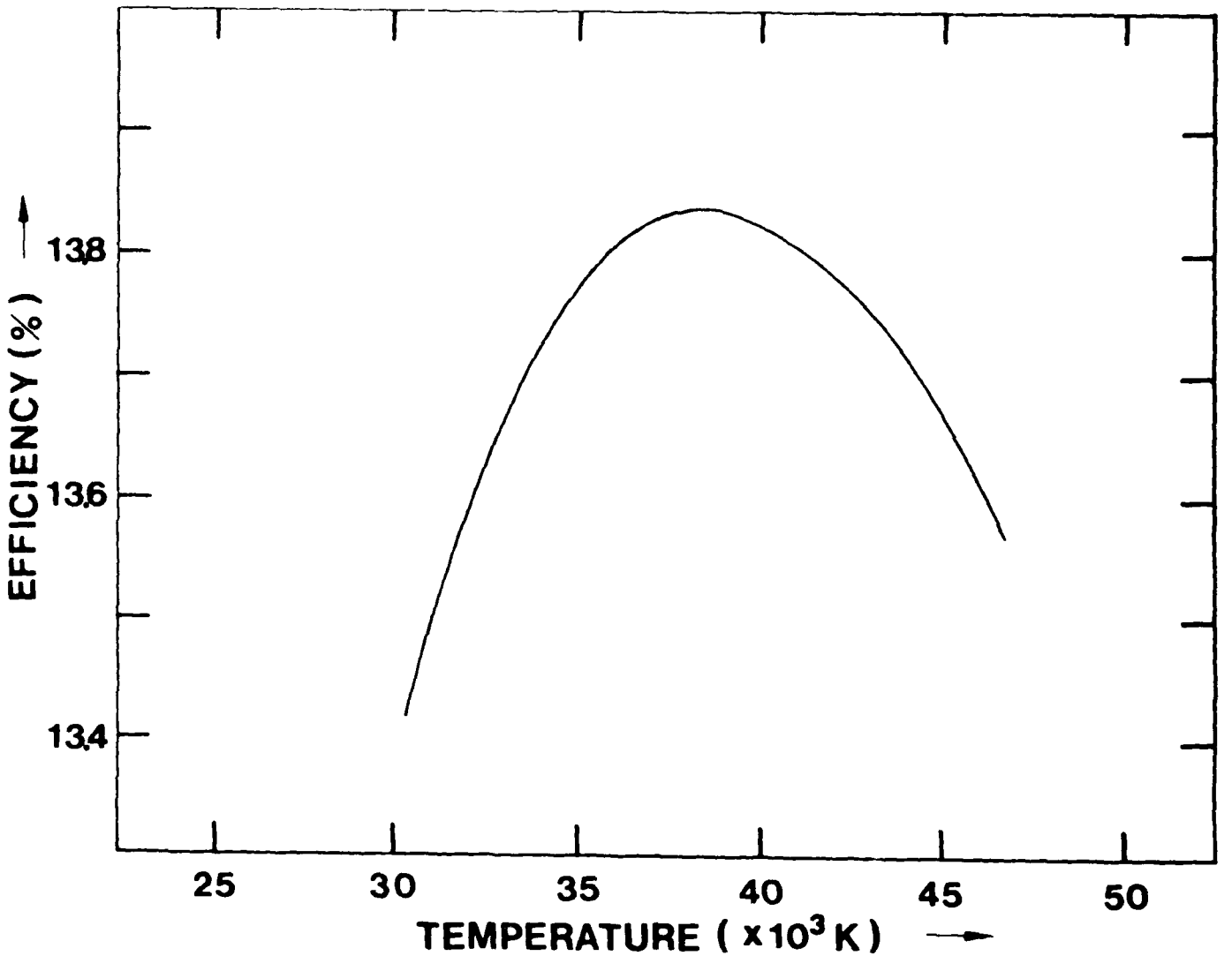

FIGURE 24. SPECTRAL EFFICIENCY OF BREMSSTRAHLUNG EMISSION FOR PUMPING LD490 AS A FUNCTION OF ELECTRON TEMPERATURE. THE ABSORPTION PROFILE OF LD490 IS TAKEN INTO THE EFFICIENCY CALCULATION.

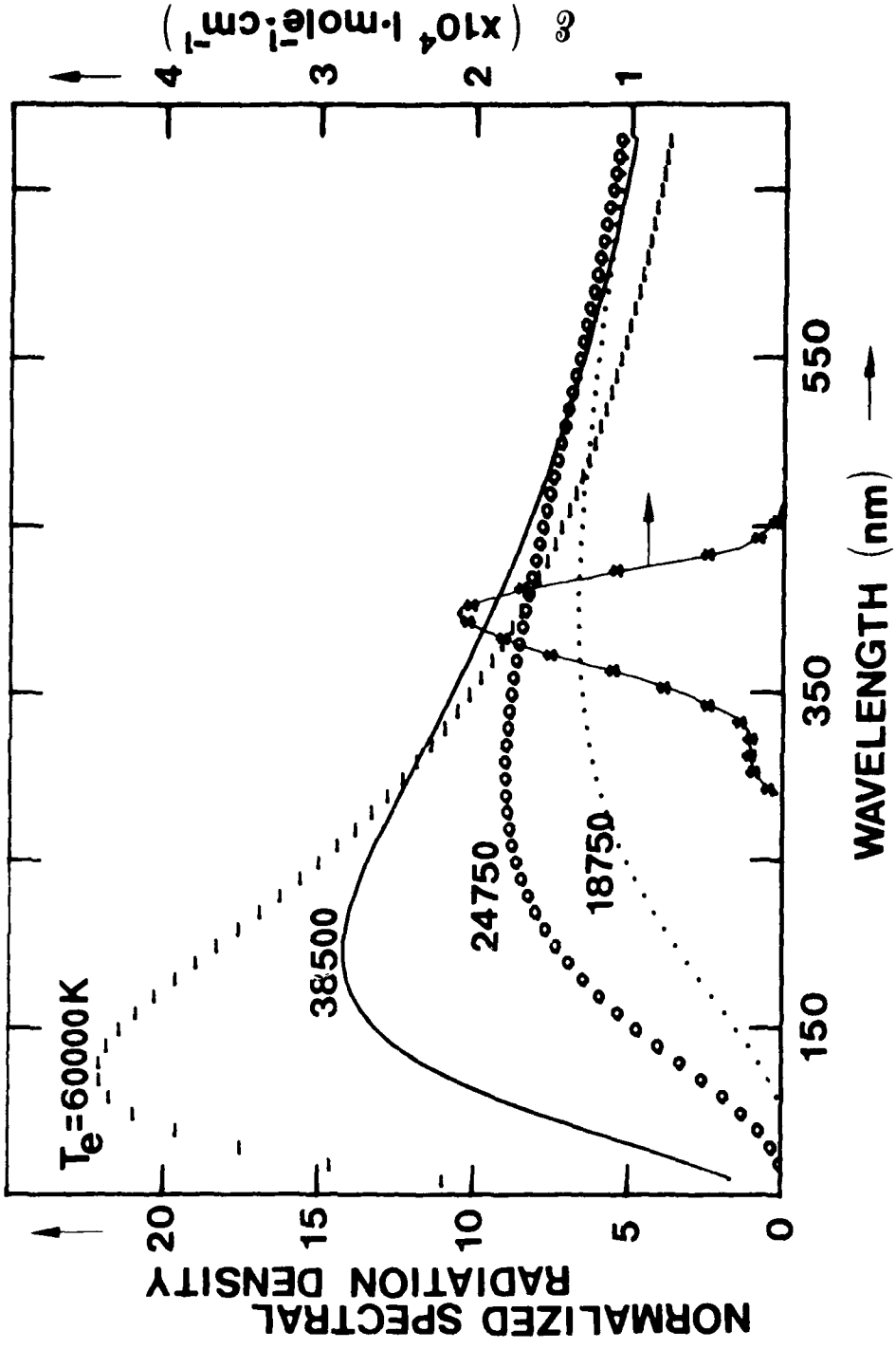

FIGURE 25. NORMALIZED SPECTRAL RADIATION DENSITIES FOR DIFFERENT TEMPERATURES AND ABSORPTION SPECTRUM OF LD490. T_{opt} IS 38,500 K. ε; MOLAR DECADIC EXTINCTION COEFFICIENT.

and the equation is as follows (Ref. 29)

$$kT_{opt} = \frac{(ch/\lambda_2)\{(\lambda_2/\lambda_1) - 1\}}{3\ \ln(\lambda_2/\lambda_1)} \tag{48}$$

However, the Equation (48) only considers a certain pump band and does not consider the dye absorption profile. With Equation (48), the optimum temperature for pumping LD490 which has absorption band (FWHM) from 370 nm to 430 nm is 12,000 K. This optimum temperature for the absorption band is different from the optimum temperature considered for the absorption profile. The rather large difference indicates that care should be taken for optimizing the pump source spectrum with the lasant absorption band.

Figure 24 shows the spectral efficiency for bremsstrahlung emission, η_{br}, as a function of T_e. For low pressure discharges the plasma is often optically thin and bremsstrahlung emission may be applied. At a temperature of 38,500 K (3.18 eV), the efficiency shows the maximum of 13.84% as shown in Figure 25. The figures shows "normalized" spectral radiance densities for several different temperatures and an absorption profile of LD490. The spectral curve is obtained by using the following equation

$$E_n = \frac{E_\lambda}{E} \tag{49}$$

where, E_n is a normalized spectral radiation density and E is the spectral bremsstrahlung emission. Figure 25 shows that E_n at the absorption spectrum builds up at the temperature increases until the optimum temperature, 38,500 K, is reached. At temperatures above optimum, E_n decreases

and thus the efficiency decreases. The peak wavelengths of E_n with temperatures of 60,000 K (5.0 eV), 38,000 K (3.2 eV), 24,750 K (2.1 eV) and 18,750 K (1.6 eV) are 130 nm, 190 nm, 300 nm, and 400 nm, respectively.

As the temperature increases, the spectral emission of blackbody radiation increases both at the short and long wavelengths. On the other hand, bremsstrahlung emission shows an increase only at short wavelengths and a decrease at long wavelengths. Therefore, the optimum temperatures for blackbody and bremsstrahlung radiation shows significant difference.

The radiation of a high-current flashlamps almost corresponds to the blackbody radiation at 8,000 K. The optimum temperature of blackbody radiation for pumping blue-green lasers is too high to obtain with flashlamps due to their low explosion energy (Ref. 11). On the other hand, the radiation from the HCP plasma operated with high pressures may be considered as a blackbody radiation and the optimum temperatures for pumping blue-green dye lasers could be achieved with proper operating conditions. The high-input power operation of HCP for obtaining optimum temperature little affects the lifetime of the all-metal HCP array. Indeed the color temperature measured was already over 7,200 K even with the limited energy source (<3 kJ) used in this experiment.

CHAPTER IV

Summary and Conclusions

A high power dye laser using LD490 and Rh6G was successfully pumped with a multiple array of hypocycloidal pinch plasmas. In the experiment, two different types of heavy filling gases in the high pressure regime were used. For the first time laser excitation was achieved by the HCP filled with high-pressure heavy gases (i.e., Xe or Ar). The untuned peak wavelength of the blue-green laser with the LD490 was 503.5 nm and the maximum output power was 230 kW with ~1 μs half-width. The maximum output energy was 163 mJ for LD490 and the maximum output energy density was 40 mJ/cm^3. A maximum overall efficiency of 0.012% was achieved using the HCP. The slope efficiency of this system was 0.004%. The overall efficiency was somewhat smaller than that for commercial flashlamp laser system (<0.25%) (Ref. 10). This difference is mainly ascribed to the impedance mismatching between the HCP and the high impedance external circuit used. However, the external circuit inductance could be significantly reduced by adopting a fast pulse power circuit for the best matching. Furthermore, a disk type capacitor bank system is custom made and placed around the HCP, the system efficiency will be improved drastically.

The optimum pressure of the filling gas was ~20 Torr. At this pressure, there was a good spectral match between the pumping light and the absorption band of LD490. By using xenon gas, 1.5 times more laser output energy was obtained as compared with argon gas. This result [illegible]

AD-A135 873 AN INTENSE EXCITATION SOURCE FOR HIGH POWER (BLUE-GREEN) LASER(U) HAMPTON INST VA DEPT OF PHYSICS AND ENGINEERING STUDIES K S HAN 22 NOV 83 2/2

UNCLASSIFIED ARO-17633.1-PH-H DAAG29-80-G-0014 F/G 20/5 NL

END

DATE FILMED

2-84

DTIC

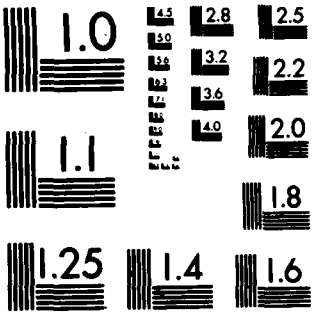

MICROCOPY RESOLUTION TEST CHART
NATIONAL BUREAU OF STANDARDS-1963-A

that using heavier gas in the HCP results in the emission of more intense light. Laser output from the laser medium inside of a quartz dye cuvette was about 1.5 times more intense than that obtained using a pyrex dye cuvette. This result is due to the fact that the absorption band of blue-green dye exists in the UV spectral region which is within the pyrex transmission cutoff region.

A dye concentration of 4.6×10^{-4} M/l was the optimum for the HCP laser pumping. In the case of flashlamp pumping, optimum dye concentration is reported to be $\sim 2.3 \times 10^{-4}$ M/l. This indicates that the HCP laser system is more suitable for high power blue-green laser pumping than flashlamp laser systems.

Input energy limitation was not found up to 4.3 kJ. It is expected that the input energy limitation is very high because the HCP laser pumping system is comprised of all metal housing, and because the plasma compression has the radial direction towards the center of the dye cuvette and it compresses the dye cuvette uniformly. Accordingly, the yielding point of the cuvette placed in the center of a HCP due to the plasma compression force is in general substantially higher than the tensile yielding point of a cuvette due to the plasma expansion from inside of the tube as in most of flashlamp configurations. The high input energy limitation means the suitability of HCP for high power blue-green laser operation.

For dye laser operation, one of the important factors is the risetime of the laser pumping source. In reality, the risetime of HCP tends to increase as molecular weight of the gas species increases, but the risetime is more significantly dependent on the external circuit para-

meters. For this reason a capacitor bank which is formed by three units of a low capacitance and high voltage (2.03 μF and 60 kV) capacitor was selected to hold the risetime to less than 1.5 μs. This was adequate for pumping the dye laser. The minimum threshold energy was achieved when 300 J of input electrical energy was used indicating one capacitor unit (maximum energy capability: 3.7 kJ) is sufficient. As a result, the risetime can be decreased by a factor of $3^{\frac{1}{2}}$, and the system efficiency can be increased substantially. Also it will be possible to operate the HCP laser system repetitively because the charging time could be reduced since the capacitance is small.

The optical threshold energy for LD490 was 11.04 J for 40% T output mirror. The threshold energies for coumarin dyes have been reported to be about 12 J with a 6% T output mirror for flashlamp pumping (Ref. 25) which is same with 40% T for HCP pumping. This may be due to the fact that the emission of the HCP source has a better spectral distribution for pumping a blue-green laser and a better coupling of the source and the dye medium.

The round trip fractional photon loss in the resonator was adjusted by selecting the output mirror transmittance. The optimum condition for the maximum laser output was obtained with a 40% output mirror transmittance.

The laser output power of LD490 is higher than with Rh6G. This result proves that the light emission of HCP in the UV is intenser than of the commercial flashlamps. The laser output of Rh6G pumped with Xe flashlamp is higher than that of LD490. Therefore, the HCP laser system is suitable for pumping blue-green and UV dye lasers.

Spectral efficiencies of blackbody and bremsstrahlung emissions were studied to obtain optimum temperatures for pumping LD490. The maximum efficiency of blackbody radiation is 26.46% at the electron temperature of 9750 K (0.84 eV). While for bremsstrahlung emission, the maximum efficiency is 13.84% at the temperature of 38,500 K (3.18 eV). Since the radiation of high-pressure HCP plasmas may be considered as blackbody emission, higher power operation is desirable for further optimization of blue-green dye pumping. The measured color temperature of the HCP array is 7,250 K when a blackbody emission is assumed. The spectral efficiency for this temperature is 22.08% or 83.45% of the maximum efficiency obtainable from blackbody radiation.

The change in the surface optical characteristics of the dye cuvette which was used in the experiment was mainly caused by the electrode-sputtering and revealed as a negative aspect. The surface of the dye cuvette is easily coated by brass vapor distilled from the brass electrode due to high plasma temperature. This coating enabled laser output energy to decrease. However, this decreasing effect was less significant than the photodegradation of dye. This coating effect would be eliminated by using high temperature metals such as tungsten, molybdenum, etc.

In conclusion the reported results make significant progress toward satisfying the goals enunciated in Table 1 for underwater communications. Future improvements of the HCP laser system may fully achieve these goals.

REFERENCES

1. Rautian, S. G., Sobel'Mann, I. I.: Opt. Spectrosc. 10, 65 (1961).

2. Brock, E. G., Czavinsky, P., Hormats, E., Nedderman, H. C., Stripe, D., Unterleitnev, F.: J. Chem. Phys. 35, 759 (1961).

3. Broude, V. L., Mashkevich, V. S., Prikhot'ko, A. F., Prokopyuk, N. F., Soskin, M. S.: Sov. Phys.-Solid State 4, 2182 (1963).

4. Stockman, D. L., Mallory, W. R., Tittel, F. K.: Proc. IEEE 52, 318 (1964).

5. Stockman, D. L.: Proc. of the ONR Conf. on Organic Lasers, Doc. no. AD 447468, Defense Documentation Center for Scientific and Technical Information, Cameron Station, Alexandria, VA, USA (1964).

6. Sorokin, P. O., Landard, J. R.: IBM J. Res. Develop. 10, 162 (1966).

7. Stopanov, B. I., Rubinov, A. N., Mostovnikov, V. A.: J. Appl. Spectrosc. 7, 116 (1967a).

8. Stopanov, B. I., Rubinov, A. N., Mostovnikov, V. A.: JETP Lett. 5, 117; Russ.: 5, 144 (1967b)

9. Handbook of Optics, edited by Walter G. Driscoll, William Vaughn (McGraw-Hill, NY, 1978).

10. White, M. B.: Opt. Eng. 16, 145 (1977).

11. Furumoto, H. W., Ceccon, H. L.: Appl Opt. 8, 1614 (1969).

12. Lee, J. H., Williams, M. D.: Bull. Am. Phys. Soc. 22, 1211 (1977).

13. Lee, J. H., McFarland, D. R.: Appl. Opt. 19, 3343 (1980).

14. Rieger, H., Kim, K.: J. Appl. Phys. 52, 5381 (1981).

15. Lee, J. H., McFarland, D. R., Hohl, F.: Phys. Fluids 20, 313 (1977).

16. Kim, K., Fanning, J. J.: CLEO '83, 144 (1983).

17. Nair, L. G.: Prog. in Quantum Electron. 7, 153 (1982).

18. Schäfer, F. P., ed., Topics in Applied Physics, Vol. 1, Dye Lasers, Springer, Berlin (1973).

19. Weider, I.: Appl. Phys. Lett. 21, 318 (1972).

20. Fletcher, A. F.: Appl. Phys. 14, 295 (1977).

21. Lee, J. H., McFarland, D. R.: Va. J. of Sci. 29, 183 (1978).

22. American Institute of Physics Handbook, 3rd ed., edited by Dwight E. Gray (McGraw-Hill, NY, 1972).

23. Data sheet 7710-f, General Electric Co. (1975).

24. Data sheet of Exciton Chemical Co. Inc., P. O. Box 3204, Dayton, OH 45431, USA.

25. Reynolds, G. A., Drexhage, K. H.: Opt. Commun. 13, 222 (1975).

26. Kodak materials for emission spectrosgraphy, 2nd ed.: Eastman Kodak Co. (1968).

27. RCA Electro Optics Handbook, RCA/Solid State Division/ Electro Optics and Devices/ Lancaster, PA 17604, USA (1974).

28. Jahoda, F. C., Little, E. M., Quinn, W. E., Sawyer, G. A., Stratton, T. F.: Phy. Rev., 119, 843 (1960).

29. Gusinow, M. A.: IEEE J. Quantum Electronics QE-11, 929 (1975).